D E S I G N A N D C A L I B R A T I O N O F A N E W A P P A R A T U S T O M E A S U R E T H E S P E C I F I C E L E C T R O N I C C H A R G E

Thesis by

George Clement Dacey

In Partial Fulfillment of the Requirements

for the Degree of

Doctor of Philosophy.

California Institute of Technology

Pasadena, California

1951

ACKNOWLEDGMENTS

The author wishes to express his gratitude for the constant and invaluable assistance of Prof. W. R. Smythe, under whose direction the following work was done. Credit and thanks are also due to Prof. H. V. Neher, Mr. Frank Silhavy, the staff of the Mount Wilson Observatory, and others too numerous to mention. The author wishes to express special appreciation to Mr. W. T. Ogier and Mr. John Lauritzen. Much of what follows is due to them, and they are in a unique position to know what the following pages represent in terms of human values.

Finally, appreciation must be expressed to the Office of Naval Research, for providing the funds which made this work possible.

ABSTRACT

The theory of a free electron method for measuring e/m_0 is described. This method consists essentially in the use of a well defined, rotating, high-frequency magnetic field as a phasing valve to determine the velocity of an electron stream. Use of the relativistically correct energy equation then yields e/m_0, if the potential of the electron stream is known. As shown below the use of a resonant cavity operating in the TM_{110} mode, approximately produces such a field.

The apparatus which was designed and constructed to support the cavity, maintain high-vacuum, provide radio-frequency, produce and measure the electron beam, and measure the parameter of interest is described. Included also are circuit diagrams of the various control and measurement electronic circuits.

Finally, data are given which determine essentially the resolving power of the instrument. Estimates are made as to the probable ultimate accuracy of the measurement. It is shown that an accuracy of 1 part in 10,000 should be easily obtainable in a given run, and that accuracies of several parts in 100,000 should be possible with more data.

TABLE OF CONTENTS.

I. The Theory of the Experiment.

1.0 General Introduction.

For many years the specific electronic charge (e/m) has been a subject of considerable interest to physicists. It remains today the most uncertain of the important physical constants, the best value being the least-squares value of DuMond & Cohen[1] who give

$$e/m = (1.758897 \pm .000032) \times 10^7 \text{ e.m.u./gr.}$$

as of 1950. The best direct measurement is the 1937 one of Dunnington[2] who quotes

$$e/m = (1.7597 \pm .0004) \times 10^7 \text{ e.m.u./gr.}$$

It is true that superior accuracy has been obtained by indirect measurements, for example the experiments of Thomas, Driscoll & Hipple[3] who give

$$e/m = (1.75890 \pm .00005) \times 10^7 \text{ e.m.u./gr.}$$

All such indirect experiments, however, measure e/m for bound electrons and are subject to inaccuracies in associated physical constants from which e/m must be derived. Then too, a derived value of any physical constant is not suitable for a least-squares adjustment of the atomic constants[1]. Clearly therefore, a new and more accurate free electron, i.e. deflection, direct value for e/m is highly desirable.

Now any deflection method for measuring e/m_0 depends upon measuring the velocity of an electron, v, which has fallen through a known potential difference, V. Application of the relativistic energy equation

$$eV = m_0c^2(1 - v^2/c^2)^{-\frac{1}{2}} - m_0c^2$$

where c is the velocity of light, will then yield e/m_0.

The present method is similar in principle to that of

---

1. J.W.M. DuMond & E.R. Cohen, unpublished report to the N.R.C.
2. F.G. Dunnington, Phys. Rev. 52, 475, (1937)
3. H.A. Thomas, R.L. Driscoll, & J.A. Hipple, Phys. Rev. 78, 787, (1950)

Kirchner[1], though quite different in detail. In a preliminary and exploratory experiment C. H. Wilts[2] investigated the possibilities of using cavity resonators to produce deflection fields. In the present experiment rotating magnetic fields are used to produce deflection, for as will be shown, a higher resolving power can be obtained than with non-rotating field deflection. An electron entering the cavity is acted upon by this rotating magnetic field during its time of transit, τ, and leaves the cavity with a transverse component of velocity which depends upon this transit time, As is shown below, if the transit time is adjusted to coincide with an integral number, n, of cycles of the parameter $k/2\pi$ ($k/2\pi$ is approximately equal to the rotation frequency, f.) then the electron emerges with no net transverse component of velocity. The cavity can accordingly be used as a sort of "phasing valve" velocity detector; for when integral cycle transit has obtained the axial, i.e. total, velocity of the electrons is approximately

$$v = d/\tau \approx df/n \qquad .....(2)$$

where d is the length of the cavity. A more accurate equation for v is obtained below.

The ultimate value of e/m_0 will, by an inspection of equations (1) and (2), be seen to depend on the measurement of: a) a voltage, V., b) a length, d, and c) a radio frequency, f.

1.1 The Equations of Motion of the Electrons.

Consider a system of rectangular cartesian coordinates with a uniform magnetic field, $B_1\sin(2\pi ft)$, in the y direction and a similar field $B_2\cos(2\pi ft)$, in the x direction. Let the electron beam

---

1. F. Kirchner, Phys. Zeits., 30, 773 (1929)
2. C. H. Wilts, Doctorate thesis, Cal. Tech. Library

be initially traveling in the z direction with the velocity v_o.

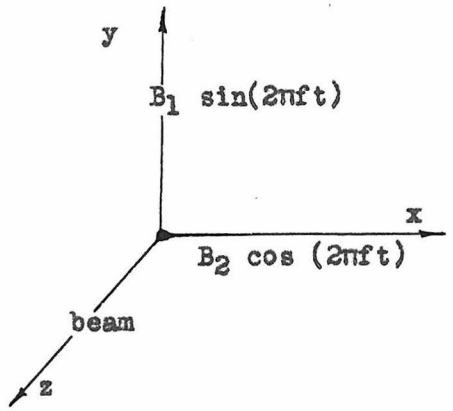

Fig. 1.

The equations of motion referred to this coordinate system, (see Fig. 1.) are:

$$\ddot{z} = -b_1\dot{x}\sin(2\pi ft) + b_2\dot{y}\cos(2\pi ft) \quad .....(1)$$

$$\ddot{x} = b_1\dot{z}\sin(2\pi ft) \quad .....(2)$$

$$\ddot{y} = -b_2\dot{z}\cos(2\pi ft) \quad .....(3)$$

Where the dot implies differentiation with respect to time and the abbreviation

$$b_i = \frac{B_i e}{mc} \quad .....(4)$$

has been employed to represent the cyclotron frequency (here in e.s.u)

1.2 Non-rotating case. ($B_1 = 0$)

If we set $B_1 = 0$ in the equations of motion of 1.1 we obtain simply a non-rotating uniform magnetic field. Clearly from Eq. (2) of 1.1 if $\dot{x}$ is originally zero it will remain so, and we shall have motion in the y-z plane. If we differentiate 1.1 (3) and eliminate $\dot{z}$ and $\ddot{z}$ we obtain

$$\frac{d(\ddot{y})}{dt} + 2\pi f \tan(2\pi ft)\ddot{y} = -b_2^2 \cos^2(2\pi ft)\dot{y} \quad .....(1)$$

Upon employing the transformation $u = \sin(2\pi ft)$, (1) becomes

$$\frac{d^2\dot{y}}{du^2} = -\frac{b_2^2}{(2\pi f)^2}\dot{y} \quad .....(2)$$

which is readily seen to have sinusoidal solutions. If we take as boundary conditions at $t = 0$; $\dot{x} = \ddot{x} = \dot{y} = \ddot{y} = 0$ $\dot{z} = v_o$

and transform the time viz: $t = nT + \theta + \phi/2\pi f$; $T = 1/f$ where ϕ measures the phase of entry of an electron and θ measures the difference between the transit time and an integral number of cycles. Then

$$\dot{y} = v_0 \sin \left\{ (b_2/2\pi f) \sin \phi + \sin 2\pi f\theta \cos \phi - \cos 2\pi f\theta \sin \phi \right\} \quad (3)$$

$$= v_0 \sin \alpha$$

Similarly,

$$\dot{z} = v_0 \cos \alpha \quad \ldots.(4)$$

So that we shall define:

$$\alpha = \tan^{-1} \dot{y}/\dot{z} = (b_2/\pi f) \cdot \sin \pi f\theta \cos (\pi f\theta - \phi) \quad \ldots.(5)$$

1.3 Shape of current peak for non-rotating field.

Consider an electron beam of width s deflected as in 1.2 and after drifting a space D being collected on a slit also of width s.

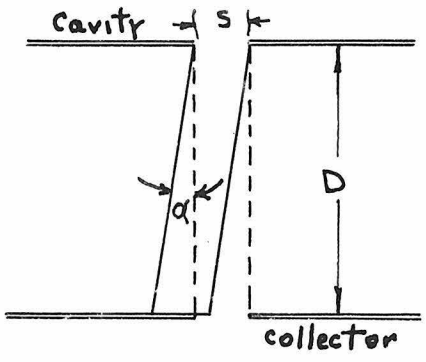

Fig. 2

(See Fig. 2.) Choosing the slit width equal to the beam width yields a sharp top to the current peak collected through the slit. Now as an inspection of Eq. 1.2 (5) will show that α varies sinusoidally in ϕ and that there consequently exist values of ϕ, i.e. phases of entry, for which $|\alpha| < s/D$. Therefore some current will be collected no matter what the transit time may be. As will be shown later, the rotating field case does not suffer from this defect. Now if θ is so small that $|\alpha| \leq s/D$ for any value of ϕ then

$$I = \int_0^{2\pi} I_0/2\pi \, (1 - \alpha D/s) \, d\phi \quad \ldots..(1)$$

where I_o is the incident current. This occurs when

$$\sin \pi f\theta \geq s\pi f/Db_2 = g \text{ say.} \qquad \ldots.(2)$$

However for θ sufficiently large we define

$$\phi_1 = \pi/2 - \pi f\theta \; ; \quad \alpha(\phi_1) = 0$$

$$\phi_2 = \cos^{-1} g/\sin(\pi f\theta) - \pi f\theta \; ; \quad \alpha(\phi_2) = s/D \qquad \ldots.(3)$$

and the current accordingly is

$$I = 4\int_{\phi_1}^{\phi_2} \frac{I_o}{2\pi} (1 - \alpha D/s)d\phi \qquad \ldots..(4)$$

Performing the integrations indicated in (1) and (4), we obtain

$$I = \frac{2I_o}{\pi}\left\{\sin^{-1}g/|\sin(\pi f\theta)| - |\sin(\pi f\theta)|/g + \sqrt{\sin^2(\pi f\theta)/g^2 - 1}\right\}\ldots(5)$$

for $|\sin(\pi f\theta)| \geq g$, and

$$I = I_o(1 - 2|\sin(\pi f\theta)|/\pi g) \approx I_o(1 - 2Db_2\theta/\pi s)$$

for $|\sin(\pi f\theta)| < g$. A plot of this current distribution is shown in Fig. 4, where it is contrasted with the current peak obtained from the rotating field calculations.

1.4 Rotating Field Case.

As we have seen, the equations of motion are given by 1.1 (1),(2), (3). We take $b_1 = b_2 = b$ thus obtaining a field rotating at angular frequency $w = 2\pi f$. If now we differentiate Eq. 1.1(1) twice and substitute for $\ddot{x}$, $\ddot{y}$, $\dot{x}$, and $\dot{y}$ from the equations of motion we obtain

$$\dddot{\dddot{z}} = -(b^2 + w^2)\ddot{z} \qquad \ldots.(1)$$

Let us denote

$$k = (b^2 + w^2)^{\frac{1}{2}} \qquad \ldots.(2)$$

and taking as boundary conditions $\ddot{x} = \ddot{y} = \dot{x} = \dot{y} = \dot{z} = 0$; $\dot{z} = v_o$ when

$t = 0$, we see that Eq. (1) has the solution

$$\ddot{z} = -\frac{b^2 v_0}{k} \sin kt \qquad \ldots.(3)$$

Or integrating,

$$\dot{z} = \frac{v_0}{k^2}(b^2 \cos kt + w^2) \qquad \ldots\ldots(4)$$

Now if we substitute this value of $\dot{z}$ into 1.1 (2) and 1.1 (3) and integrate we will obtain

$$\dot{x} = -\frac{wbv_0}{k^2}(1 - \cos kt)\cos(wt) + \frac{bv_0}{k} \sin kt \sin(wt) \quad \ldots(5)$$

$$\dot{y} = -\frac{wbv_0}{k^2}(1 - \cos kt)\sin(wt) - \frac{bv_0}{k} \sin kt \cos(wt) \quad \ldots.(6)$$

And if we further define

$$\dot{r} = \sqrt{\dot{x}^2 + \dot{y}^2} = \frac{bv_0}{k}\sqrt{\frac{w^2}{k^2}(1 - \cos kt)^2 + \sin^2 kt} \quad \ldots(7)$$

Note that $\dot{y} = \dot{x} = \dot{r} = 0$, when $t = 2n\pi/k$, so that current peaks similar to those of 1.3 may be expected when this condition is satisfied.

1.5 Theoretical Equation for e/m_0.

Suppose that the rotating field of 1.4 is produced in a resonant cavity of length d so that the field is confined to approximately[1] this length. If then the transit time is adjusted until $t = 2n\pi/k$ we have

$$d = \int_0^{\frac{2n\pi}{k}} \dot{z}\, dt = \int_0^{\frac{2n\pi}{k}} \frac{v_0}{k^2}(b^2 \cos kt + w^2)\, dt \doteq 2n\pi v_0 w^2/k^3 \quad \ldots(1)$$

---

1. An investigation into the amount of bulging into the hole in the end of the cavity where the electron beam enters, and of the effect of this bulging on the electron trajectory is being carried on by Prof. W. R. Smythe. This effect will bring in a small correction upon the value of e/m_0 as experimentally determined, but this correction can be calculated with extreme precision.

where V_0 is such as to fulfill the transit time condition mentioned above. We accordingly obtain as the entering velocity for a current peak

$$\overline{v}_o = \frac{bk^3}{2n\pi w^2} = \frac{d(b^2 + w^2)^{\frac{3}{2}}}{2n\pi w^2} \qquad \ldots.(2)$$

Therefore, for a given current peak, if V is the beam voltage, we have

$$eV = m_o c^2 (1 - v^2/ c^2)^{-\frac{1}{2}} - m_o c^2 \qquad \ldots.(3)$$

or

$$e/m_o = \frac{c^2}{V}\left\{1 - \frac{d (b^2 + w^2)^3}{4n^2\pi^2c^2}\right\}^{-\frac{1}{2}} - \frac{c^2}{V} \qquad \ldots.(4)$$

It is to be noted that $b = Be/mc$ is itself a function of e/m_o; however, as $b \ll w$, this will not affect the obtainable accuracy. In order to eliminate contact potentials etc., it is probably preferable to use the voltage difference $(V_2 - V_1)$ between two successive current peaks, in which case

$$e/m_o = \frac{c^2}{V_2 - V_1}\left[\left(1 - \frac{d^2(b^2 + w^2)^3}{4n^2\pi^2c^2}\right)^{\frac{1}{2}} - \left(1 - \frac{d^2(b^2 + w^2)^3}{4(n+1)^2\pi^2c^2}\right)^{\frac{1}{2}}\right] \ldots(5)$$

1.6 Deflection of the Electon Beam.

If we perform a further integration of the equations 1.4 (5) and (6), we will obtain

$$x = -\frac{v_o}{b}\left[\frac{b^2}{k^2} + \left(1 + \frac{w^2}{k^2}\right)\cos kt\right] \sin wt + \frac{2wv_o}{bk} \sin kt \cos wt \ldots(1)$$

$$y = \frac{v_o}{b}\left[\frac{b^2}{k^2} + \left(1 + \frac{w^2}{k^2}\right)\cos kt\right] \cos wt + \frac{2wv_o}{bk} \sin kt \sin wt - \frac{2v_o}{b} \ldots(2)$$

Let us define

$$r^2 = x^2 + y^2$$

Then differentiating we obtain

$$\frac{d}{dt}(r^2) = 2x\dot{x} + 2y\dot{y} = 0 \quad \text{at } t = 2n\pi/k \text{ since } \dot{x} = \dot{y} = 0 \text{ here.}$$

Furthermore after a second differentiatinn and after substituting for the values of $\dot{x}$, $\dot{y}$, etc. at $t = 2n\pi/k$ we have

$$\frac{d^2}{dt^2}(r^2) = -4v_o^2(1 - \cos wt) < 0$$

Therefore r is a <u>maximum</u> at $t = 2n\pi/k$. This maximum value is given by

$$r_{max} = (x^2 + y^2)^{\frac{1}{2}}\Big|_{t = 2n\pi/k} = \frac{4v_o}{b}\sin\frac{n\pi w}{k} \qquad ...(3)$$

Note that this result is independent of n approximately, for if we assume that $b << k \approx w$, so that $w/k = \sqrt{1 - b^2/k^2} \approx 1 - \frac{1}{2} b^2/k^2$ and that $\sin n\pi w/K \approx (-1)^{n+1} \frac{n\pi b^2}{2k^2}$ we obtain

$$r_{max} \approx \frac{2n\pi b v_o}{k^2} \qquad ....(4)$$

or substituting for v_o from 1.5 (2) we finally obtain

$$r_{max} \approx \frac{dbk}{w^2}$$

which is independent of n. This comes about because although an additional deflection is produced each cycle that the electron is in the cavity, the deflection is less <u>per</u> cycle the larger n, as this corresponds to smaller v_o for fixed d. The above results will be given numerical values later in the report when design

considerations are discussed.

1.7 Shape of Current Peak in Rotating Field Case.

Consider an electron beam of circular cross section and of diameter s, which is collected by a circular orifice also of diameter s, located a distance D from the cavity. Figure 2 above applies equally well to this case. Suppose now that the beam spent a time τ in the cavity. It accordingly leaves with a transverse velocity $\dot{r}$, given by 1.4,(7), with $t = \tau$. Its axial velocity is given by 1.4,(4). Therefore for all those electrons which enter the cavity at some particular time there is produced at the collecting orifice a displacement R of the beam given approximately by

$$R = \frac{D\dot{r}}{l_2} = \frac{Dkb\left[w^2/k^2(1 - \cos w\tau)^2 + \sin^2 k\tau\right]^{\frac{1}{2}}}{b^2 \cos k + w^2} \quad \ldots . (1)$$

Electrons entering the cavity at some different moment but having the same transit time will suffer the same displacement but in a different direction. Figure 3 shows a typical moment at the collector. The cross hatched area is that over which the beam is actually being collected. It is to be noted that the beam displacement which was mentioned in section 1.6 would alter the above results; (namely by displacing the beam into a ring, at the collector.) This effect is removed, however, by locating the collimating slit at the entrance to the final

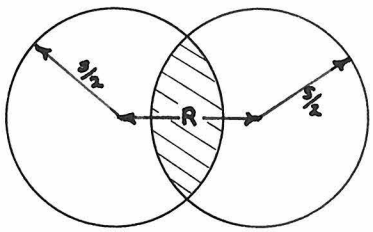

Figure 3.

drift length tube, rather than at the entrance to the cavity. A somewhat larger aperture is placed at the entrance to the cavity in order to reduce the number of electrons passing through, but this is made large enough so that it does not constitute the limiting aperture of the system.

Now the collected current is for $R < s$

$$I = I_o \frac{\text{cross hatched area}}{\pi s^2/4}$$

$$= \frac{2I_o}{\pi}\left\{\text{arc cos } (R/s) - \frac{R}{s}\left(1 - \frac{R^2}{s^2}\right)^{\frac{1}{2}}\right\}$$

$$= I_o\left\{1 - \frac{2}{\pi}\left[\text{arc sin}(R/s) + \frac{R}{s}\left(1 - \frac{R^2}{s^2}\right)^{\frac{1}{2}}\right]\right\} \quad \ldots (2)$$

And for $R < s$

$$I = 0$$

For values of τ sufficiently removed from nT, $R > s$, and thus the current actually goes to zero. This current distribution is plotted in Figure 4 as is that of 1.3(5), the non-rotating case. In both cases the field strengths chosen are close to those actually used in the experiment. It can be seen that the rotating field case yields the sharper peak. It must be remembered however that it takes twice the R.F. power to produce a rotating field of a given strength than a stationary one. The principal advantage of the rotating field case is its circular symmetry with consequent lack of cross-fire electrons.

The above calculations assume an idealized current distribution, but as will be seen in section III, the experimental results are in fair agreement.

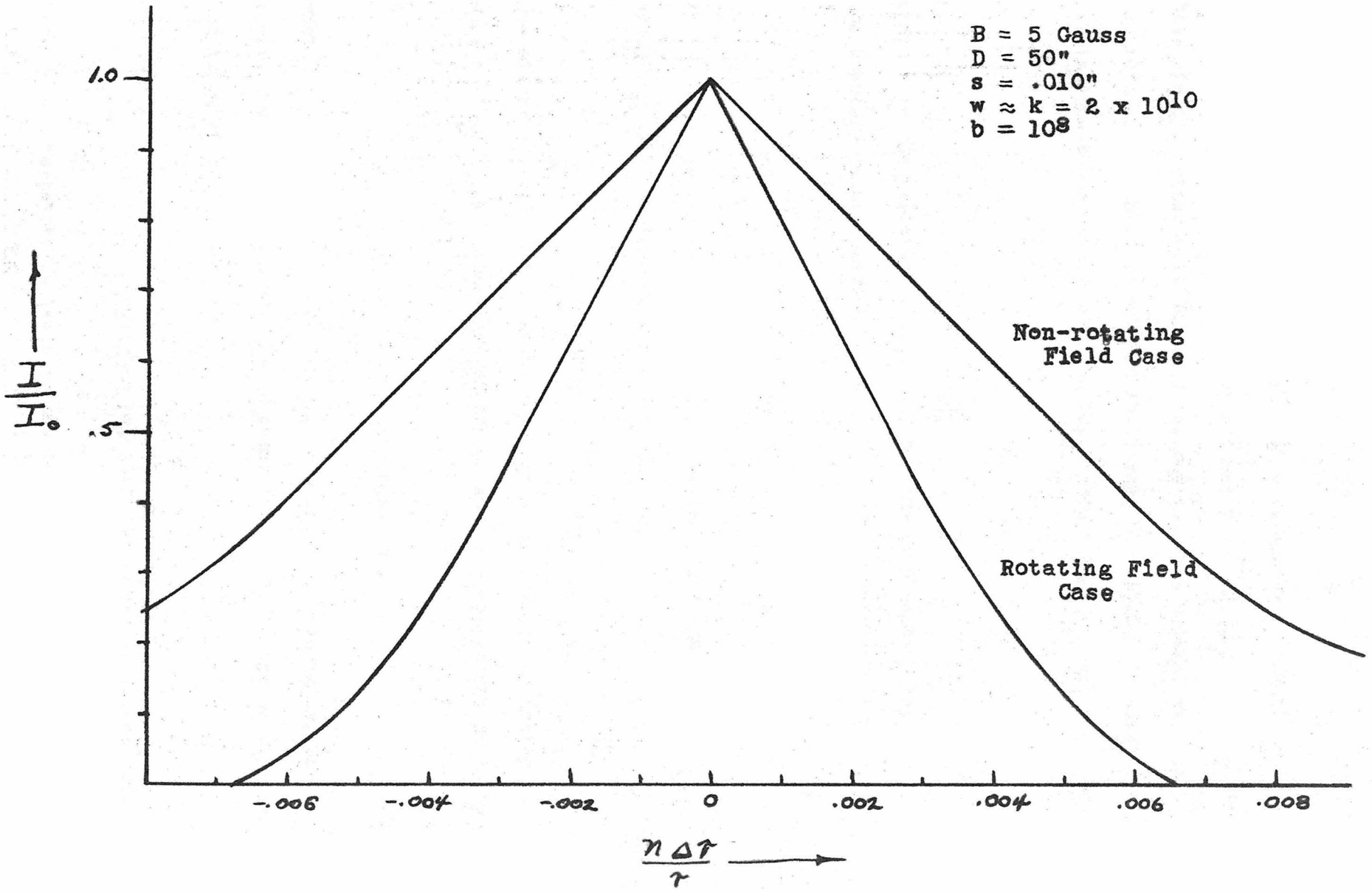
B = 5 Gauss
D = 50"
s = .010"
w ≈ k = 2 x 10^10
b = 10^8
Non-rotating Field Case
Rotating Field Case
1.0
.5
I/I₀
-.006
-.004
-.002
0
.002
.004
.006
.008
nΔτ/τ

Figure 4.

1.8 Considerations of Cylindrical Cavity in the TM_{110} Mode.

The following results have been taken from "Static and Dynamic Electricity" second edition, by W. R. Smythe. The general results are to be found there in section 15.17 page 534, &535. We have specialized those results for the TM_{110} mode. The resonant frequency of a right circular cylindrical cavity is given by

$$w = 2\pi f = c\beta$$

where c is the velocity of light and β, the wave number, obeys the boundary value relation

$$J_1(\beta a) = 0$$

where a is the radius of the cavity. Taking the 3.832 root of J_1 and using 2617 megacycles for f, yields

$$2a = 13.9736 \text{ cm.} = 5.487 \text{ inches.}$$

The electric field in the cavity has only a z, component, (using ρ, ϕ, z, the usual cylindrical coordinates), and is given at resonance by

$$E_z = wc'\beta^2 J_1(\beta\rho)\cos(\phi)\sin(wt)$$

where c' is an arbitrary constant which measures, essentially, the power input to the cavity. The magnetic field lies in the ρ-ϕ plane and is given by

$$\vec{B} = -\beta^2 c'\left[\frac{\vec{\rho}}{\rho} J_1(\beta\rho)\sin(\phi) + \vec{\phi}\beta J_1'(\beta\rho)\cos(\phi)\right]\cos(wt)$$

The "Q" of the cavity is given by the formula which follows. In this

formula δ, and γ' are respectively the skin depth and the surface R. F. conductivity.

$$Q = \frac{c\mu\delta\gamma' d\, a\beta}{2(a+d)} = \frac{ad\mu}{\mu'\delta(a+d)}$$

where μ' is the permeability of the cavity wall. For our cavity $\gamma' = 4.8 \times 10^7$ Mhos/meter, using the value for copper, and $\delta = +0.073/\sqrt{f}$ meters. The length d, is 3.063 cm. This yields

$$Q = 14{,}800$$

As chromium and molybdenum[1] are somewhat more resistive than copper the actual Q should be about 10,000. The relation between magnetic field strength at the center of the cavity and input power is

$$P = \frac{c^2(\beta a)^2 [J_0(\beta a)]^2 d}{\mu Q f} B^2$$

If we insert the numerical values already obtained above, we obtain, putting B here in Gauss, the handy working formula

$$P = \frac{20{,}000}{Q} B^2 \approx 2 B^2$$

for a Q of 10,000. That is it takes 2 watts to produce one Gauss of non-rotating magnetic field at the center of the cavity.

The magnetic field configuration described by the formula above has been plotted and is shown in Figure 5a. The lines shown are those which surround equal amounts of flux.

---

1. See section 2.2

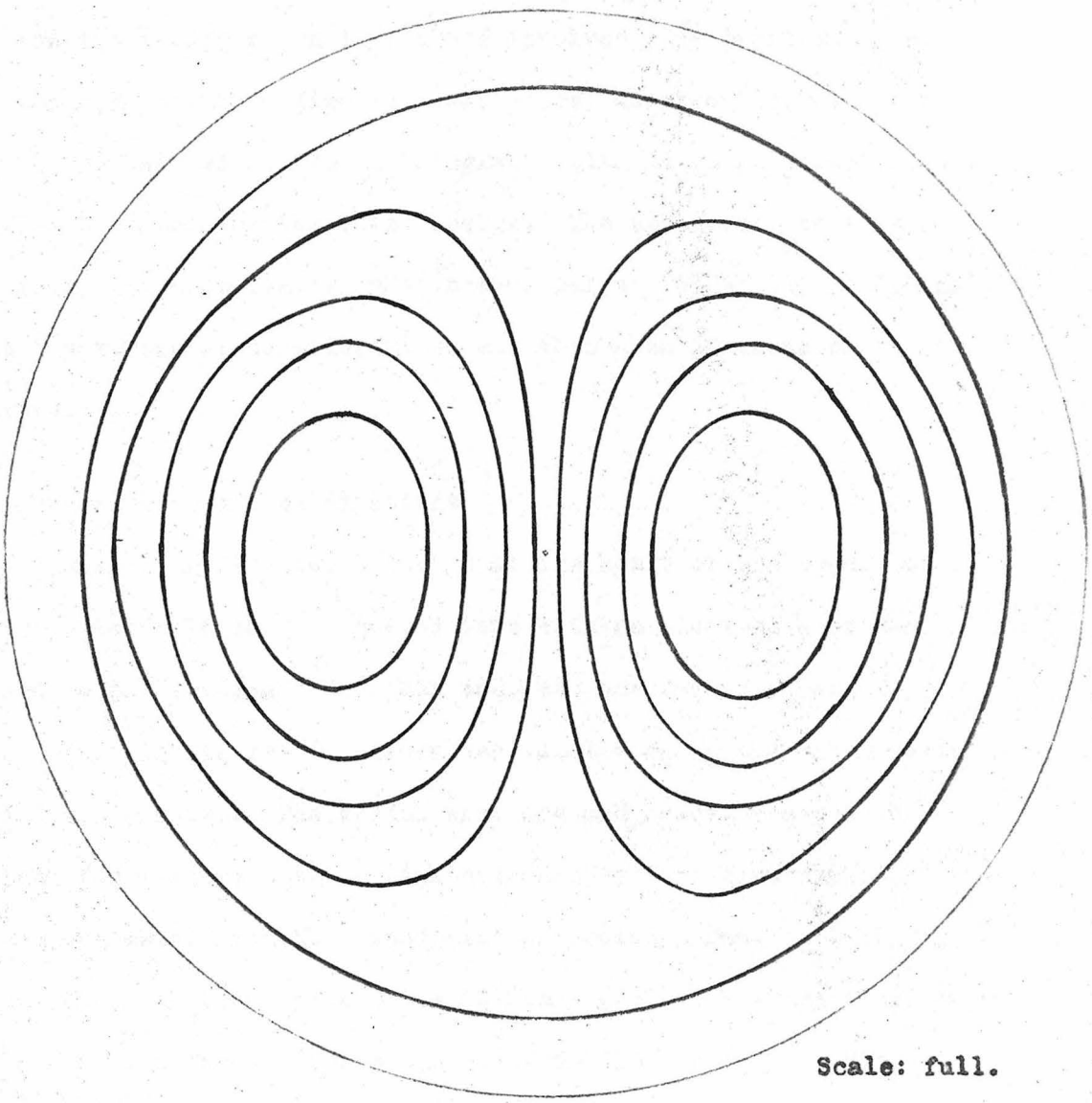

Scale: full.

Figure 5a. Magnetic Field Distribution in Cavity.

II. The Design of the Apparatus.

2.0 Introduction.

The equipment necessary to carry out a measurement of e/m_0 based on the theory given in I above involves many problems of vacuum, Radio Frequency , Electron Ballistics, electronics, etc. An attempt was made to obtain an integrated plan in which these factors combined to determine the final design. The apparatus consists of four main, and essentially independent, parts. We shall, accordingly, first treat general considerations and then each of these parts separately.

2.1 General Design Considerations.

It was clear from the outset that the heart of the apparatus would consist of a long evacuated tube with an electron source at one end, a collector at the other end, and the cavity somewhere in between. In figure 6, a cross sectional view of the final design arrived at is shown. The vacuum envelope and header are made of aluminum for reasons both of lightness and because aluminum is a good vacuum metal from the standpoint of occluded gas. All of the vacuum joints in the envelope use "O-ring" seals. ("O-rings" are a seamless molded rubber ring available from The Los Angeles Plastic and Rubber Products Co.) Metal to metal aluminum joints are arc welded. Type 51ST Alcoa aluminum was used as it is the most readily weldable of the aluminum alloys. We were perhaps fortunate that no vacuum leaks occurred in the welds. Immediately inside of these aluminum tubes are a series of six concentric tubes made alternately

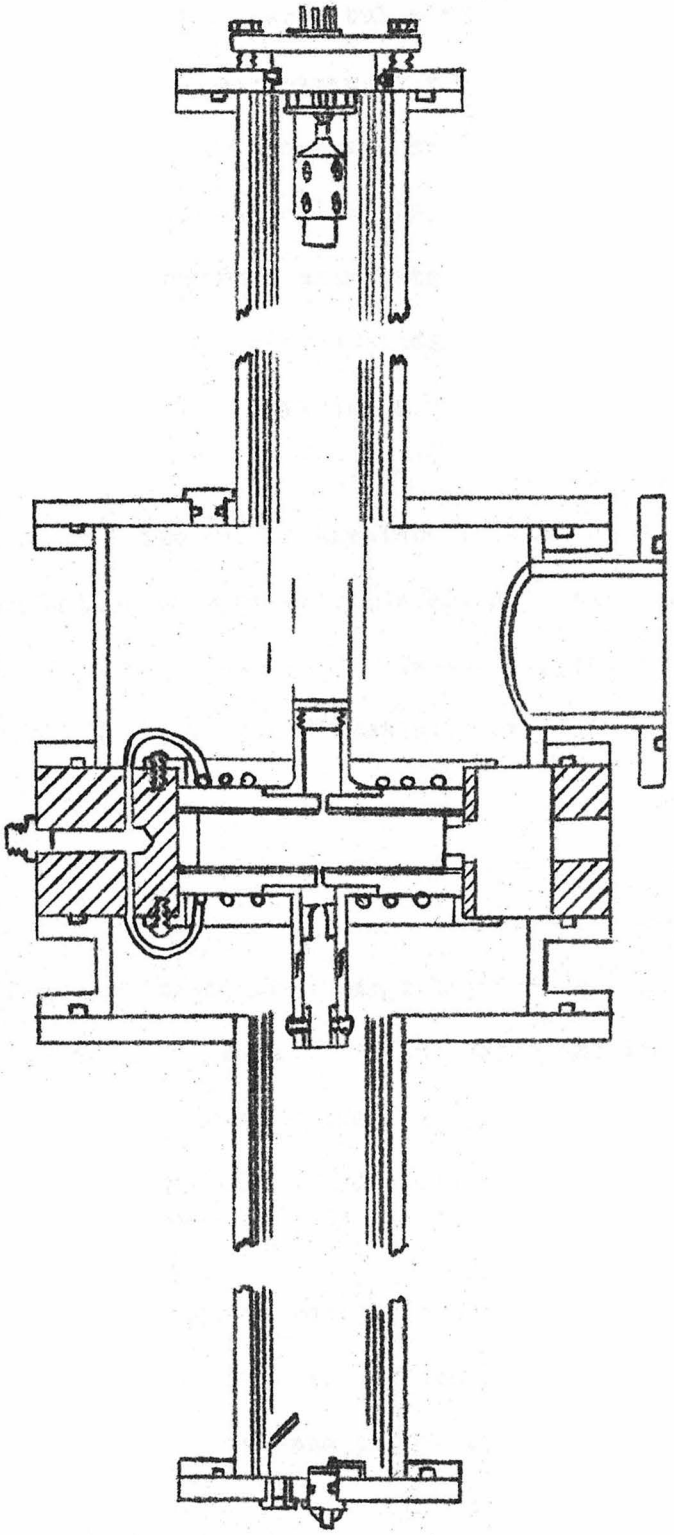

Scale: $\frac{1}{4}$" = 1"

Figure 6. Overall view, cross section.

of Mu-metal and copper. As Mu-metal has an enormous permeability these tubes form an excellent magnetic shield. This shielding is necessary not only to remove the field of the earth but also to screen out all a. c. magnetic fields. In order to minimize the virtual vacuum leaks arising from the space between the concentric cylinders of the shield, radial holes were drilled through the cylinders, (although in different locations in each cylinder in order to eliminate magnetic "leaks"). The cavity region is shielded with soft iron cylinders, not shown. In use these cylinders are demagnetized by applying a strong 60 cycle a.a. magnetic field.

The entire structure of the vacuum envelope is supported on the vacuum header which is bolted to a brass plate which in turn is bolted to a wooden framework as shown in Figure 7. Tests have shown that the geometrical alignment of the apparatus is satisfactory with no additional support.

2.2 The Cavity Section.

The cavity is supported inside of a large brass ring (see figure 8) which also serves as a header for cavity cooling water and is drilled to provide a vacuum pumping area around the cavity. The cavity itself is made in three pieces, two end plates and a spacing ring. These pieces must be optically flat in order that the cavity length can be accurately determined. It is planned that this measurement will be made by interferometric methods. It must also be possible to remove some 200 watts by water cooling. The end plates of the cavity were made from $\frac{1}{2}$" copper plate and electroplated on one side with an .020" layer of chromium. Chromium has the same electrical conductivity as

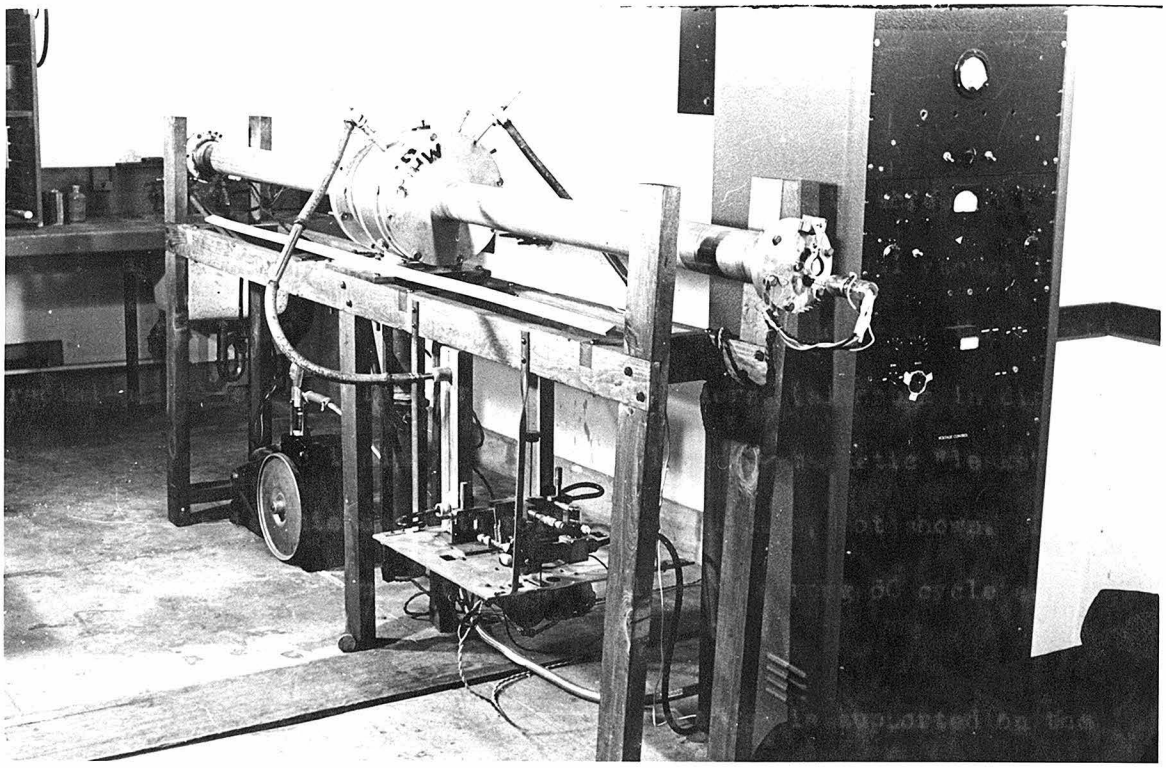

Figure 7.

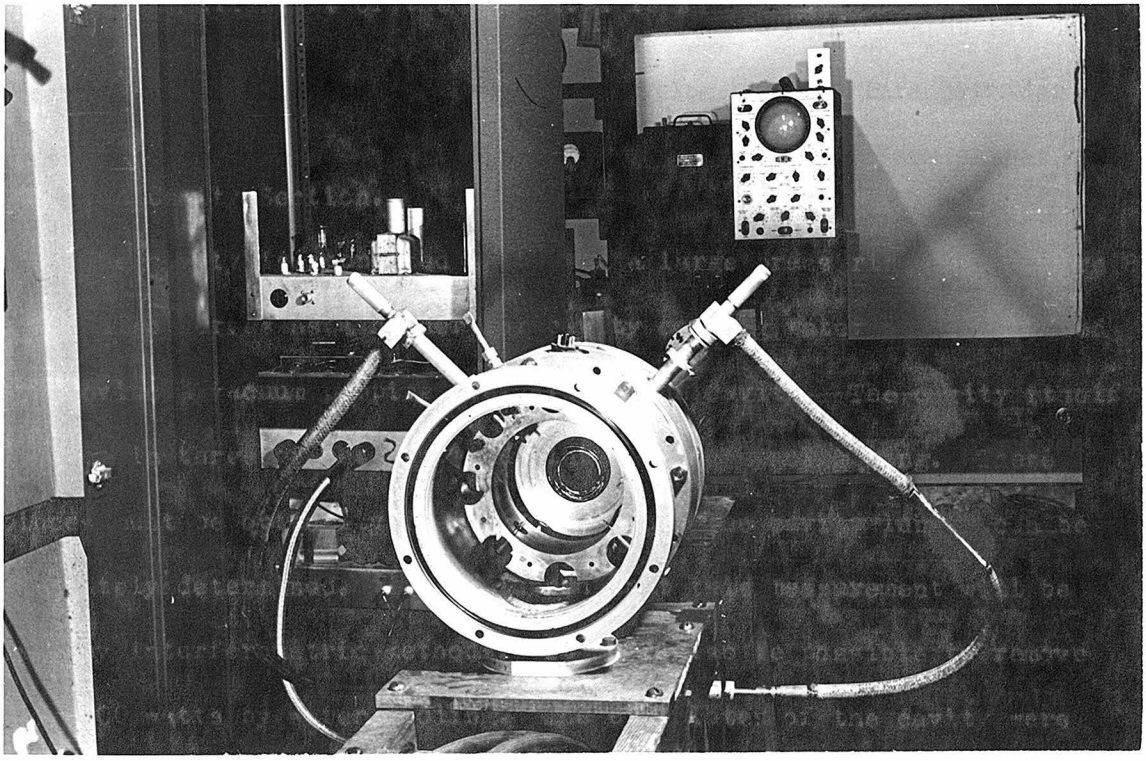

Figure 8.

gold and the scratch hardness is the same as for sapphire. It is therefore an ideal material for polishing and also makes a suitable cavity wall. Copper cooling pipes were soldered to the rear of these copper-chromium plates and they were then polished to an optical flat by the optical shop of the Mount Wilson Observatory. The spacing ring for the cavity was made of molybdenum, for that metal has the most advantageous ratio of thermal conductivity to coefficient of expansion. Appendix I. contains a calculation which shows that sufficient cooling is obtained by conduction to negate any changes in length due to expansion.

The cavity is shown assembled in Fig. 9a and disassembled in Fig. 9b Note the holes in the spacing ring through which the R.F. power is coupled to the cavity, and the deflection plates which are mounted in a lucite cylinder.

At either end of the cavity and bolted to the end plates are threaded cylinders which hold the collimating holes. This provides a well aligned structure and insures that the electron beam passes through the center of the cavity. Both of the end plates and the spacing ring are a tight fit in the brass support ring and are pressed together by spring loaded flanges. The aluminum tubes of the envelope are bolted to the brass spacing ring and in this way the entire structure is aligned.

2.3 The Electron Source.

The electron gun design finally employed is shown in Fig. 10. This structure consists simply of a diode with an orifice in the anode. It is mounted in such a way that it can be tilted by adjusting screws

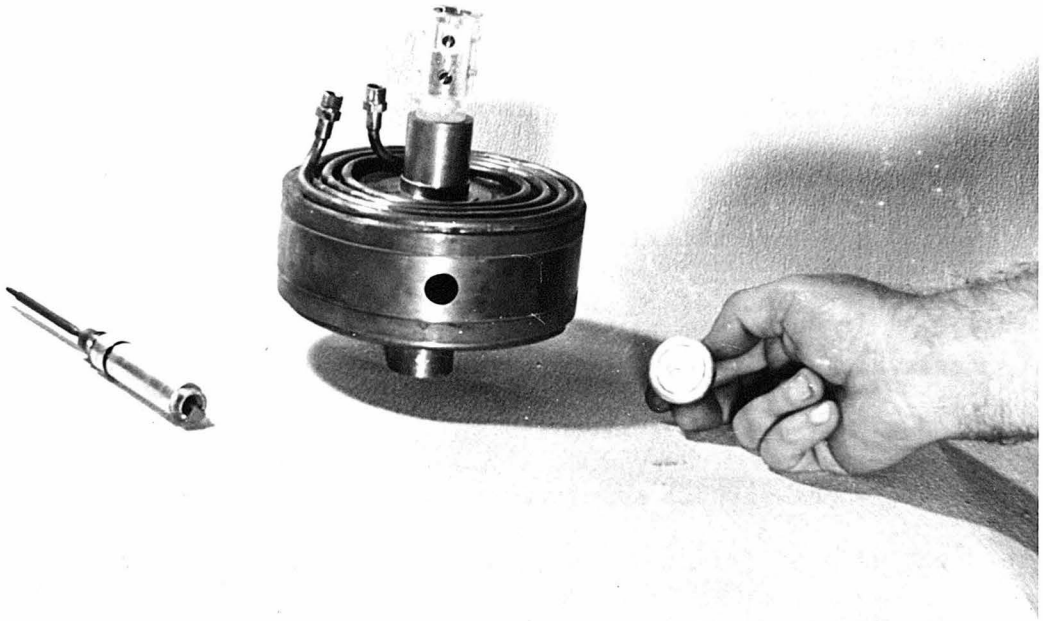

Figure 9a.

Figure 9b.

about an axis through the O-ring which seals it to the system. In an earlier model deflecting plates were used but these gave trouble due to charging and were finally entirely eliminated. The anode consists (as can be seen in Fig. 10) of a plate and attached tube of stainless steel which provides a space free of electric fields over the first few inches of the electron path. The cathode plate consists of a punched plate of stainless steel again attached to a stainless steel tube concentric to the anode tube for purposes of alignment. The insulators used are Isolantite. The shape of the cathode-anode structure has been calculated by J.R. Pierce[1] to give a parallel beam in the cathode-anode region. The cathode itself is a nickel stamping coated with Barium Oxide and indirectly heated by a tungsten heater. This cathode is of the standard type used by R.C.A. in their cathode-ray tubes, and we are indebted to Dr. H.V. Neher for kindly providing us with a supply. Unfortunately no suitable heating filaments were obtainable commercially and so the filaments which we use are wound from 0.006" tungsten wire in the form of a helix. They are coated with alumina by sintering. They operate at about 2 amperes at 9 volts and do not seem to produce objectionable magnetic fields.

It is possible to operate an oxide coated cathode at about 1200 ^{o}K. This is several hundred degrees cooler than the temperature necessary for even a thoriated tungsten filament and consequently the spread in thermal energies of the emitted electrons is correspondingly reduced.

In Fig. 11, is shown the circuit employed to supply a regulated voltage to the electron gun. A three stage, battery stabilized regul-

---

1. J.R. Pierce: The Production of Electron Beams. John Wiley & Sons.

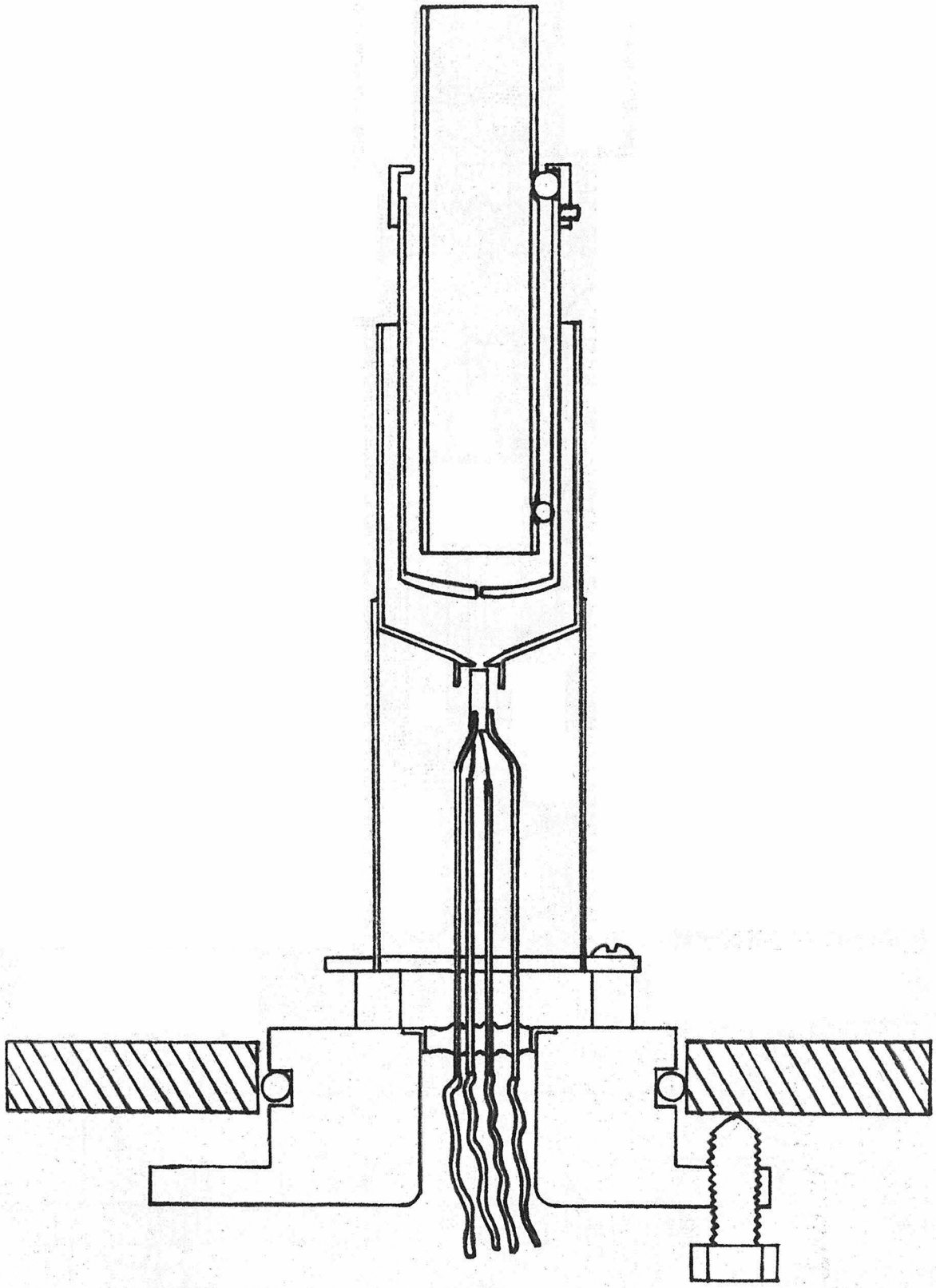

Figure 10. Electron Source.

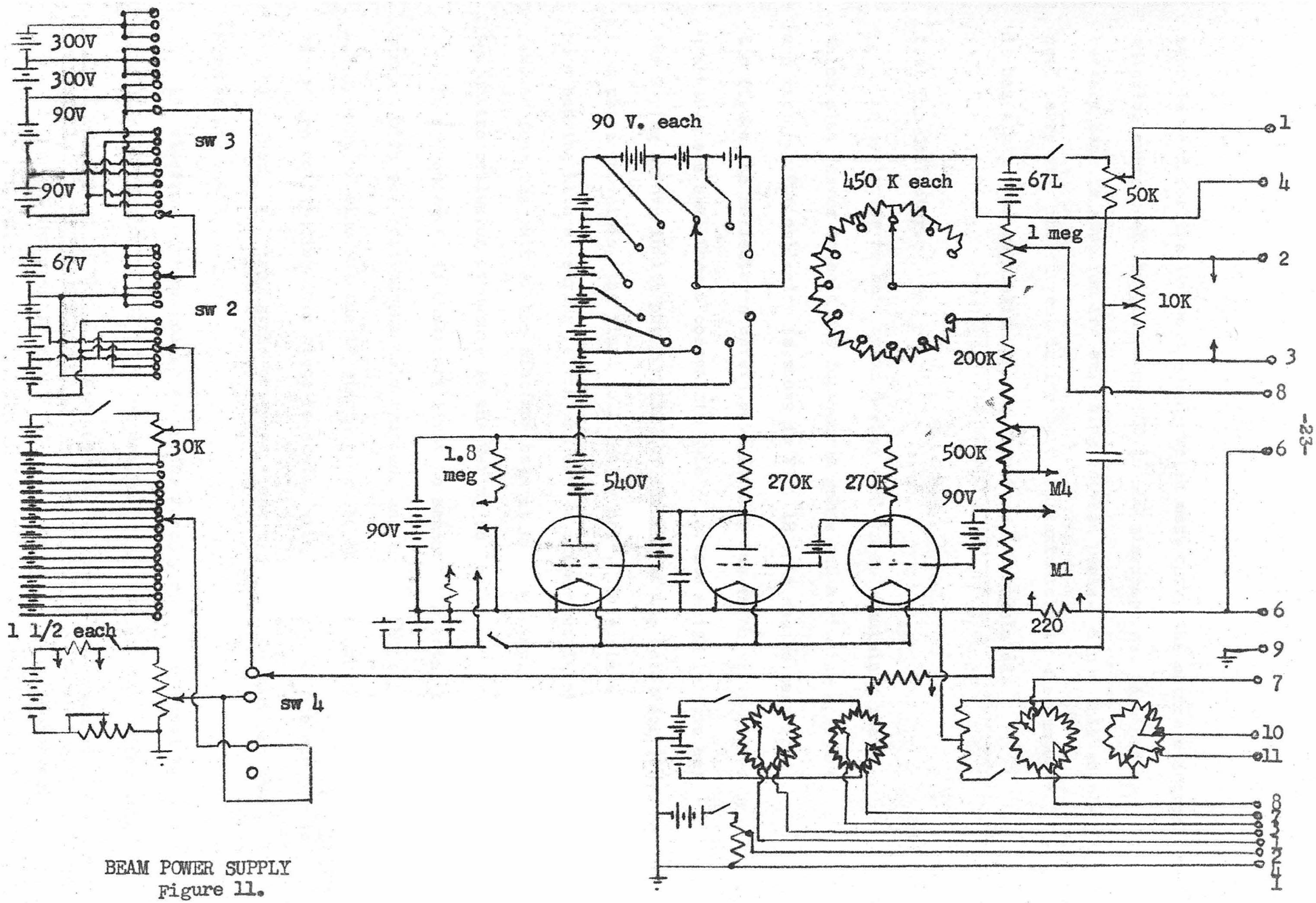

BEAM POWER SUPPLY
Figure 11.

ator is used for the 1000 volt supply which must carry the entire electron emission current of the gun--some 200 to 500 microamperes. A boosting battery bank is supplied for switching between peaks. Since this supply need carry only the current in the beam (approximately 10 microamperes.) it has small load regulation and is therefore not regulated.

2.4 The Collector.

The collector is held by an O-ring seal in an alumiminum plate which also serves to hold the ion vacuum gauge and a viewing aperture and mirror. The collector is shown in Fig. 12. As can be seen from the figure the collector consists of a Faraday cup which is insulated by a Kovar-glass seal from a concentric shielding tube which in turn has the O-ring groove in its outer wall. At the end of the collector tube is a plate containing the final collimating hole. This plate is mounted on a bearing with a spring return and can be either put in place or removed from the path of the electron beam at will by simply rotating the entire collector structure in the O-ring seal.

In operation it is customary first to measure the total beam current with the collimating hole removed, and then with it in position. A tiny spot of zinc sulfide is placed close to the hole and the remainder of the collimating hole plate is coated with Willemite. One can locate the hole then, by aligning the phosphorescent zinc sulfide spot and the fluorescing electron spot.

The electron current collected in the Faraday cup is measured by a D. C. amplifier of rather standard design. The circuit diagram for this amplifier is given in Fig. 13. The 954 tube is operated at reduced filament current for greater stability. In operation the collector and

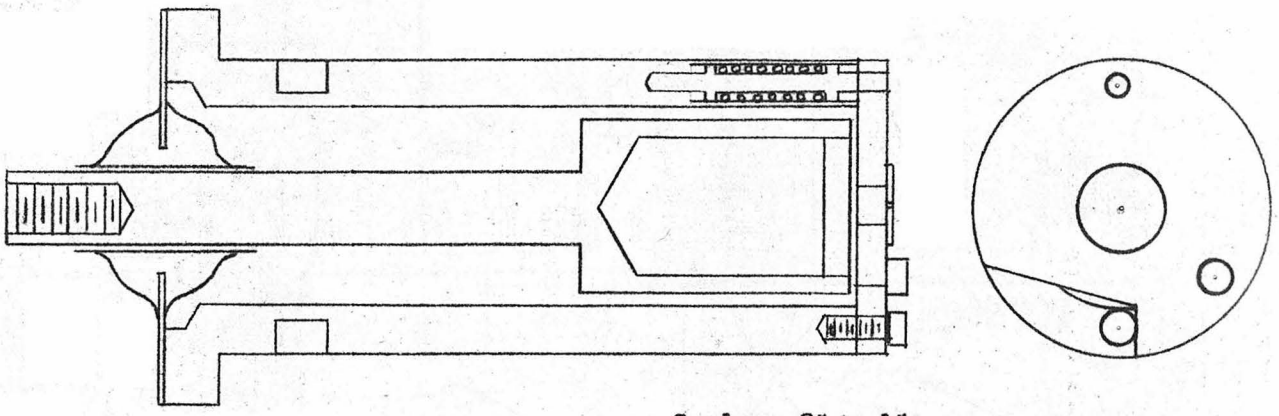

Scale: 2" = 1"

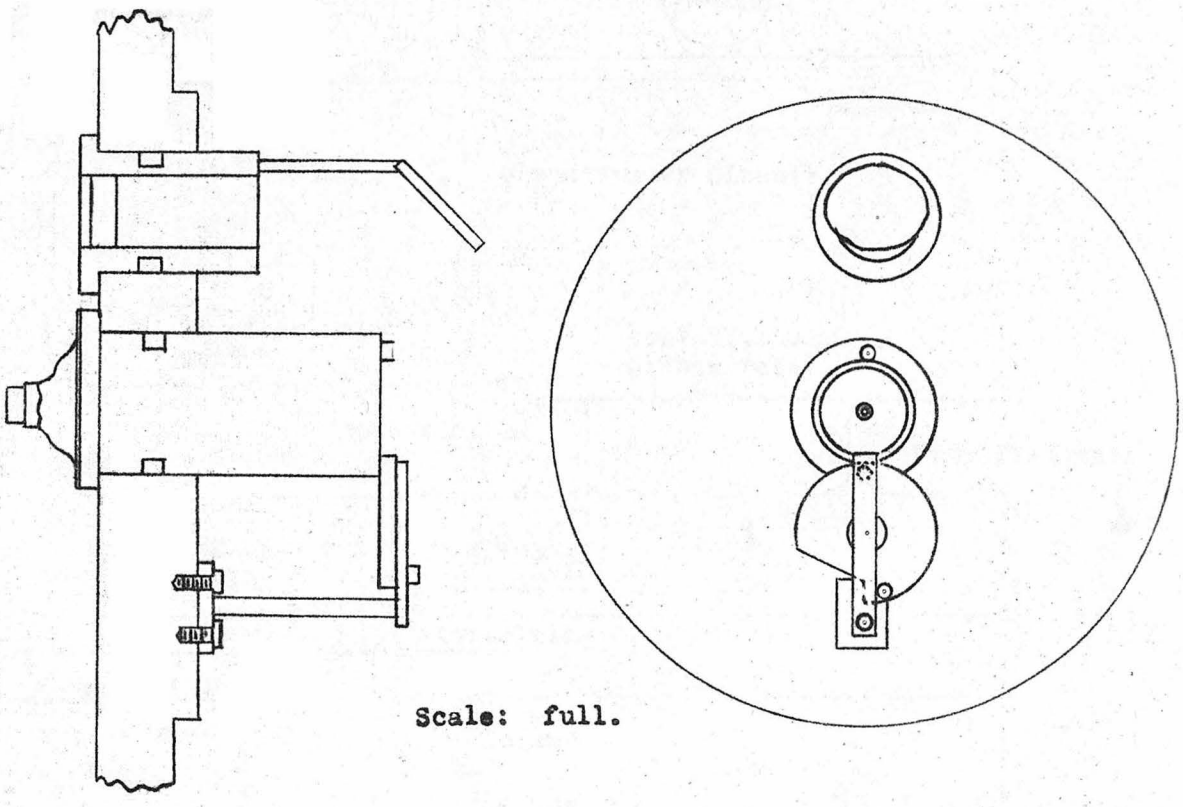

Scale: full.

Figure 12. Collector

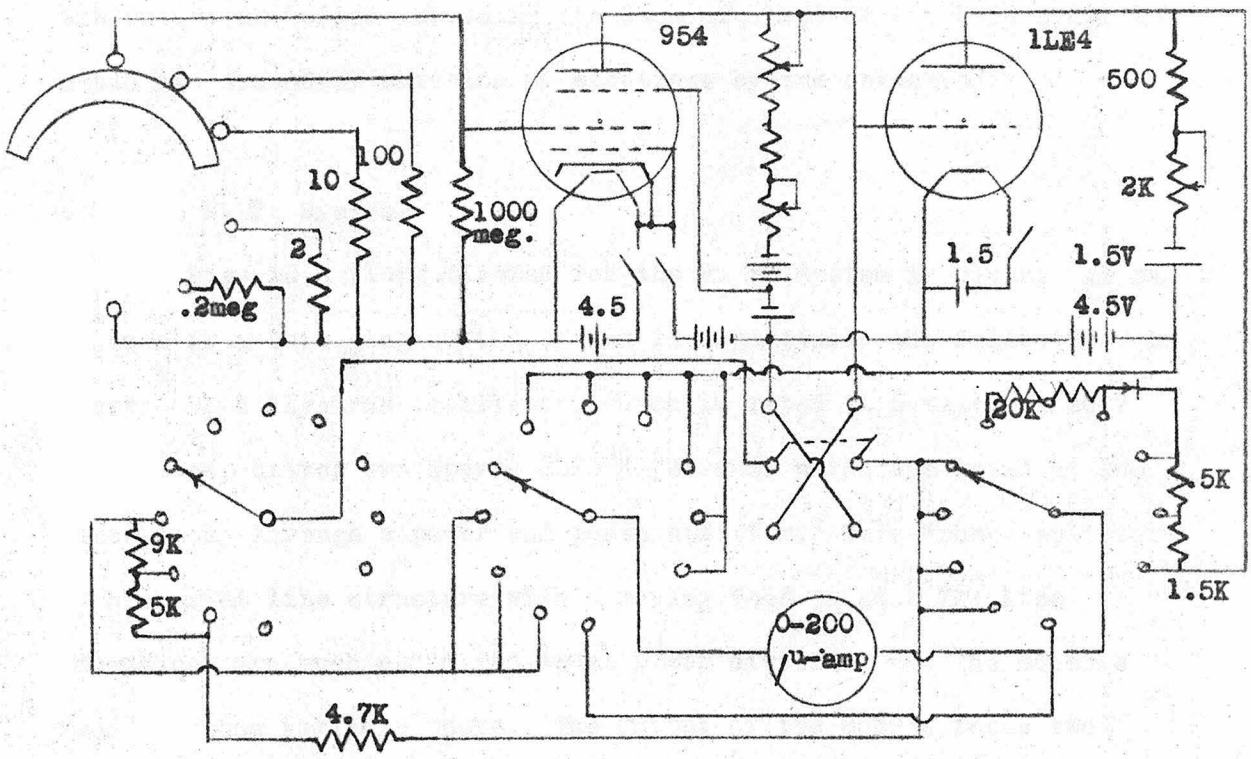

Figure 13. Electrometer Circuit.

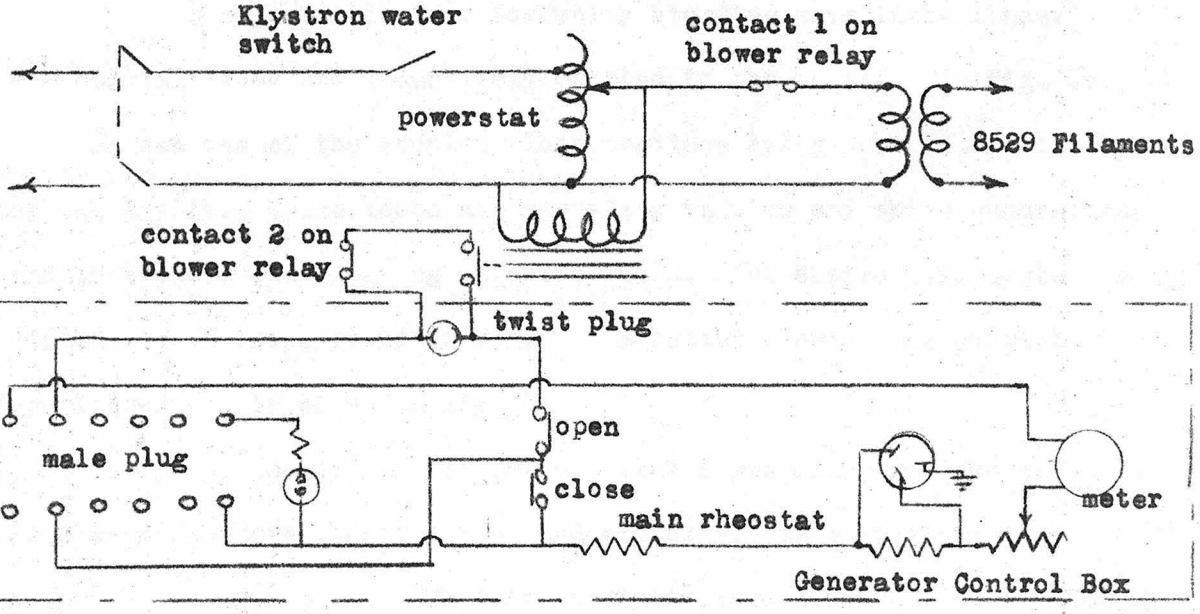

Figure 14. Klystron Protective Circuit.

the entire amplifier including its case are kept at +45 V in order to avoid the secondary emission of electrons by the collector.

2.5 The R. F. System.

In Fig. 15 a block diagram for the R. F. System is given. As can be seen from this diagram the system is essentially the following. A Sperry SRL-6 Klystron oscillator, which is rated at 5 watts at 2617 megacycles, drives two Sperry 8529 Klystrons, which are rated at 100 watts each, through a power and phase splitter. This "phase-splitter" is a coaxial line structure with a moving feed point. The line impedances are such as to get equal power division, and the movable feed provides variable phase. The output of the 8529's feeds two wave guide sections which are in turn coupled by means of probes to coaxial lines. All of the lines of the system are provided with stub tuners and slots for standing wave detection. In operation it is necessary to adjust all stubs for unity standing wave inthe lines. The coaxial lines are inductively coupled to the cavity. In Fig. 9a one can see one of the coupling loop sections lying just to the left of the cavity. These loops are operating in time and space quadrature and thus yield the rotating magnetic field. The entire R.F. system is visible in the foreground of Fig. 7. A better view of the coaxial coupling lines is shown in Fig. 8.

The power supply for the SRL-6 Klystron was made from two war-surplus dynamotors placed end to end and driven as generators by an external one h.p. motor. This arrangement gives two 1000 volt at 300 MA sources as well as two 28 V d.c. sources at 10 amp. each. One of these

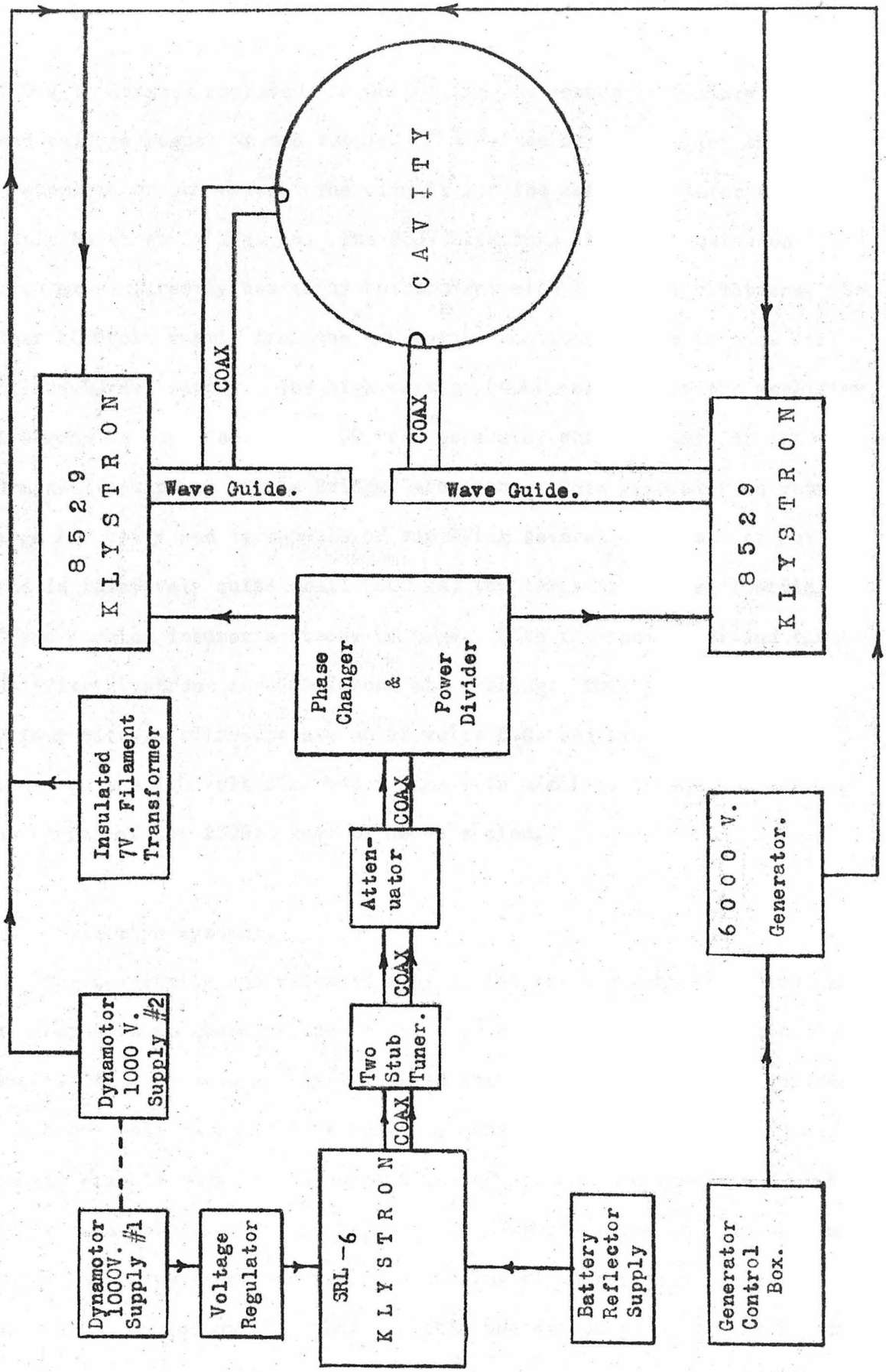
CAVITY
COAX
COAX
8529 KLYSTRON
Wave Guide.
Wave Guide.
8529 KLYSTRON
Phase Changer & Power Divider
Insulated 7V. Filament Transformer
Atten-uator
COAX
Two Stub Tuner.
COAX
SRL-6 KLYSTRON
COAX
Dynamotor 1000 V. Supply #2
Dynamotor 1000V. Supply #1
Voltage Regulator
Battery Reflector Supply
60000 V. Generator.
Generator Control Box.

Figure 15.

1000 volt sources operates the SRL-6 Klystron through a battery stabilized voltage regulator and supply. The reflector voltage for the SRL-6 is supplied by batteries. The circuit for the SRL-6 regulator and supply is shown in Fig. 16. The 8529 Klystrons have disc cathodes which are indirectly heated by bombardment with 1000 volt electrons. The other 1000volt supply from the dynamotors mentioned above is used for this bombarder supply. The high voltage (4000 volts.) for the amplifier Klystrons is supplied by a 6000 volt generator which is part of the permanent equipment of the Bridge Laboratory. This generator is very large and heavy and is capable of supplying several amperes. As our load is relatively quite small (600 MA) the large rotational inertia of the machine insures a steady voltage. Both the oscillator and the amplifier Klystrons require forced air cooling. This is supplied by four blowers which operate on 28 volts D.C. and are operated in series on the 110 volt d.c. house line. In addition to the air cooling the anodes of the 8529's must be water cooled.

2.6 Protective Systems.

The complexity and value of many of the parts of the apparatus make it imperative to guard various components of the system from accidental damage. We have accordingly installed the following protective devices.

A possible water failure could, in the case of the vacuum system, deposit cracked pump oil throughout the apparatus. In the case of the Klystrons a water failure during operation would irreparably damage the tubes. We have therefore put interlocking water switches in the exhaust lines of the cooling water to both the oil pump and to the Klystrons. In the case of the oil pump this switch turns the pump power off in

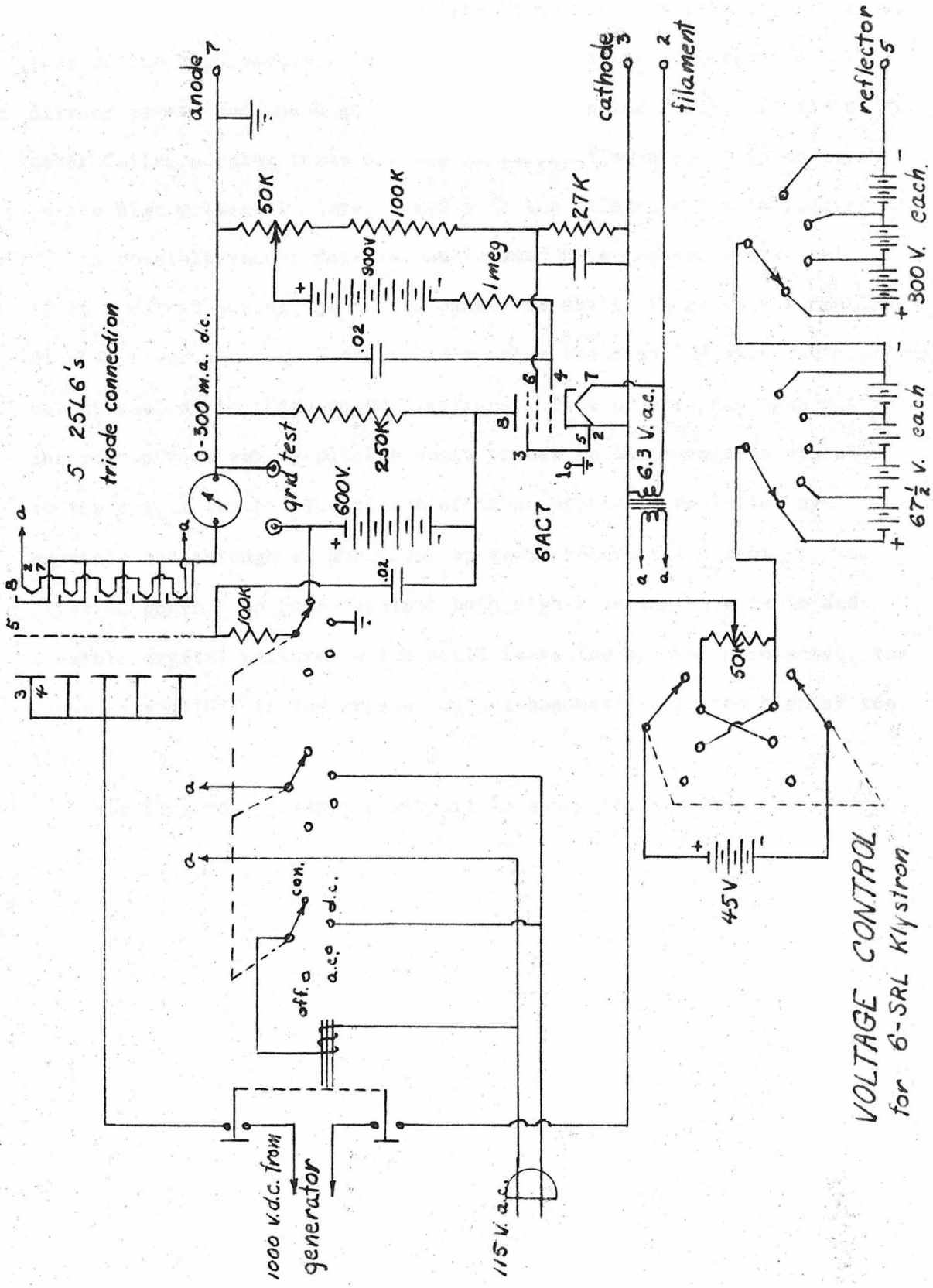
5 2516's
triode connection
anode
cathode
filament
reflector
0-300 m.a. d.c.
grid test
600V.
250K
100K
50K
100K
27K
900v
1 meg
.02
.02
.02
6AC7
6.3 V. a.c.
45 V
300 V. each
67½ V. each
off
a.c.
d.c.
com.
1000 v.d.c. from generator
115 V. a.c.
VOLTAGE CONTROL
for 6-SRL Klystron

Figure 16.

the event of water failure, thus permitting the pump to cool before the loss of the high vacuum. The Klystron water switch removes the R.F. driving power, and the high voltage when the water fails. If the blower power fails, a relay turns off the Klystron filaments, In as much as the high voltage is interlocked with the filaments, it is removed also.

A possible vacuum failure, say caused by a cracked glass seal, might if it occurred during operation, cause the cavity to go into a continuous discharge and would thus dangerously raise the standing wave ratio at the output seal of the high power Klystrons. This problem has been met in the most direct way by placing small probes in the waveguide opposite to the output seals. The pickup of these probes is rectified by crystals and through an amplifier operates relays which shut off the Klystron power. To guard against both high standing wave ratio and possible crystal failure, which would leave the system unprotected, the power is shut off if the crystal output becomes either too high or too low.

The Klystron protective circuit is shown in Fig. 14.

III. Experimental Results and Conclusions.

3.0 Introduction.

In this section we shall describe the experimental results obtained and draw conclusions therefrom which bear upon the ultimate accuracy of the measurement of e/m. At this stage of the experiment, however, we had not as yet set up the apparatus for the precise measurements of voltage, frequency and length referred to at the end of 1.0. These results, therefore, will yield only estimates as to the resolving power of the instrument, and will permit estimates as to the ultimate accuracy of the actual e/m measurement when it is made.

3.1 Experimental Results--Current Peaks.

Typical measured current peaks, of the type predicted in section 1.7, are shown in Fig.17 and Fig. 18. It will be convenient in describing these curves to define the term "half-width" to mean the change in beam voltage necessary to reduce I/I_0 from 1, its value at the synchronous voltage, to 0.5. It is essentially therefore, the familiar, "half width at half maximum."

It is clear from an inspection of Eq. 1.7,(1),&(2), that the shape of the current peaks depends on a large number of parameters. It must be remembered too, that the theoretical peak shapes derived in section 1.7 and shown in Fig.4, are based on an idealization of the current distribution in the beam. Actually, the beam does not have a uniform "disc" of intensity, but, rather, exhibits an umbra and penumbra, characteristic of the illumination of one hole through another. It is somewhat surprising therefore, that the agreement between the theoretical curve of Fig. 4

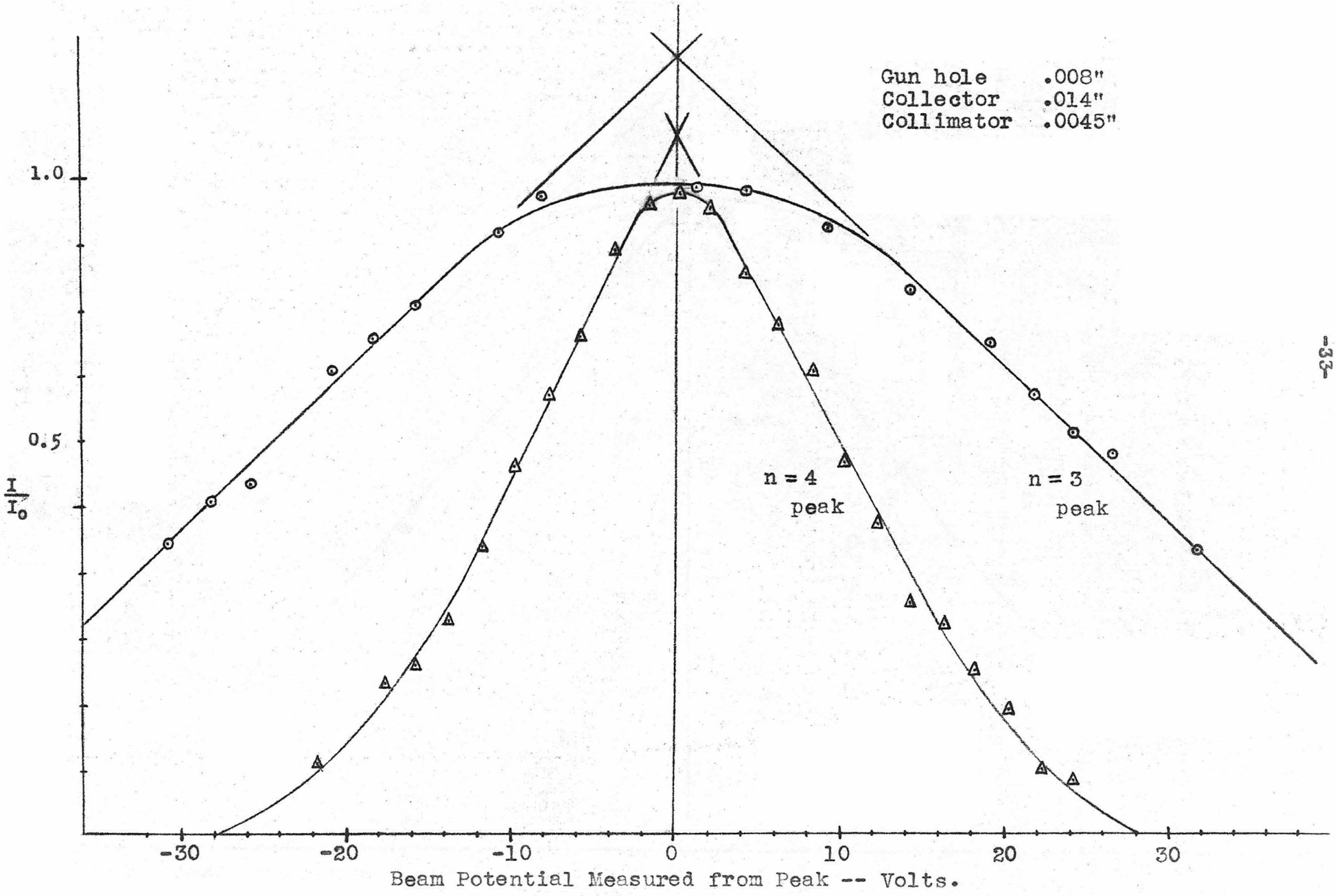
Gun hole .008"
Collector .014"
Collimator .0045"
1.0
0.5
I/I0
n = 4
peak
n = 3
peak
-30
-20
-10
0
10
20
30
Beam Potential Measured from Peak -- Volts.

Figure 17.

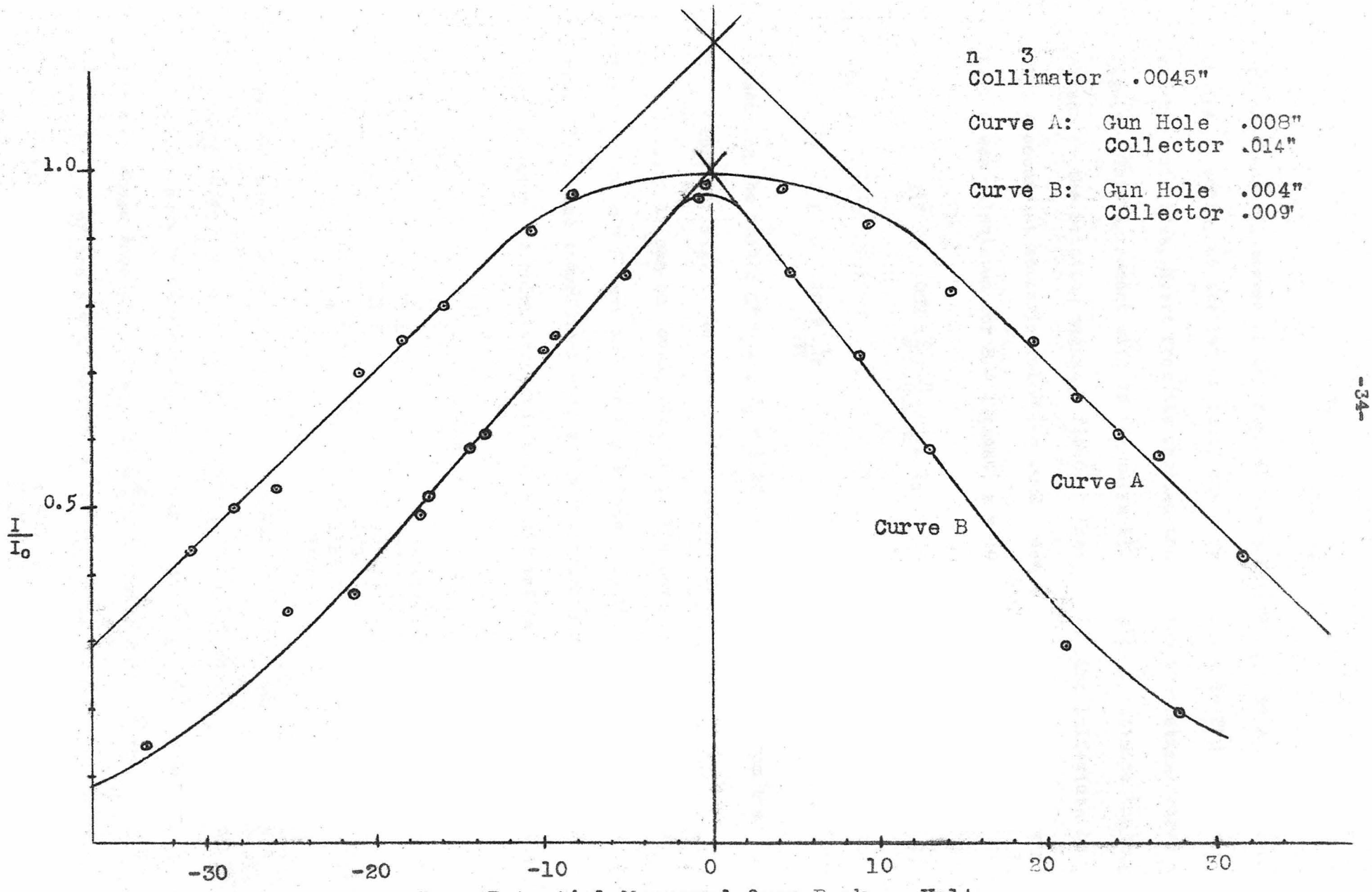
n 3
Collimator .0045"
Curve A: Gun Hole .008"
Collector .014"
Curve B: Gun Hole .004"
Collector .009"
1.0
0.5
I/I0
Curve A
Curve B
-30
-20
-10
0
10
20
30
Beam Potential Measured from Peak -- Volts.

Figure 18.

and the measured curves of say Fig. 17, is so striking. By a fortuitous choice of scale, as amatter of fact, the curve of n = 4 in Fig. 17 almost exactly coincides, apart from its rounded top, to the theoretical curve of Fig. 4. This agreement with theory makes it possible to estimate the magnitude of the rotating magnetic field in the cavity. The half-width in Fig. 4 occurs at approximately $\eta\frac{\Delta\tau}{\tau} = .002$. Now since $\frac{\Delta\tau}{\tau} = \frac{1}{2}\Delta V/V$, and since Fig. 4 was calculated for B = 5 gauss, s = .010" we obtain

$$\Delta V = .002 \times \frac{5}{B} \times \frac{s}{.002} \times \frac{2}{n} \times V_0 = 10\,\frac{sV_0}{nB}$$

or,

$$B = 10\,\frac{s}{n}\,\frac{V_0}{\Delta V}$$

Inserting the values $\Delta V = 12$, $V_0 = 1125$ (see table I below) from the n = 4 curve of Fig. 17 we obtain B = 3.3 Gauss.

In Fig. 17 can be found, plotted to the same scale, current peaks for both the n = 3 case and the n = 4 case. In the following table we have listed the theoretical values for the synchronous voltages in the various cases, as calculated from the relativistically correct Eq. 1.5,(4)

TABLE I.

n	V_0(volts.)
2	4575.4
3	2006.2
4	1125.6
5	719.5

where the accepted present value of e/m has been inserted, Since these voltages range over a large scale, one would expect the half-widths of different peaks to vary considerably. In fact, as all curves are of the same shape when plotted against $n\frac{\Delta\tau}{\tau}$, the half width of the n = 3 peak and that of the n = 4 peak should be in the ratio

$$\frac{\Delta V_3}{\Delta V_4} = \frac{4\,V_3}{3\,V_4} = \frac{4 \times 2006.2}{3 \times 1125.6} = 2.38$$

The measured half widths, as can be seen from Fig 17, are 28 volts for the n = 3 peak, and 12 volts for the n = 4 peak. These are in the ratio of 2.34 which compares very favorably with the theoretical value.

The voltage measuring equipment used for these measurements, while giving fairly accurate changes in voltage, did not give the absolute values of V_o. Voltage variations were obtained by setting the 500K potentiometer of Figure 11. This potentiometer was a Beckman Helipot, and is linear to ½%. It was felt however, that part of the scatter of points might be due to drift in the beam potential and therefore a crude voltage divider and type K, Leeds and Northrup, potentiometer, in the usual voltage bridge circuit was used as a check. This voltage was indeed found to drift from time to time, and the use of the type K improved the scatter somewhat. It was also possible with the type K, set-up to check at least roughly, the voltage V_o, of the peaks. In the following table these rough results are given

TABLE II.

n	V_o(theoretical)	V_o(measured)
3	2006.2	2054
4	1125.6	1157

The fact that these do not agree is not significant, firstly, because the voltage divider used was made up out of 1% resistors, and secondly because the effect of cavity bulging fields has not been included. (See footnote 1 section 1.4) Since both values are high, however, this may give evidence that the cavity bulging fields tend to <u>increase</u> the effective length of the cavity. It can be shown, that to first order, there is no correction necessary when either the hole is very small at the entrance to the cavity

or when the cavity end plate is very thin. There is no a priori reason therefore to expect the correction to be in a given direction.

3.2 Effect of Beam Size.

It can be seen from an inspection of Eq. 1.4,(2) that the half-width of a given peak depends almost linearly on R/s. It is desirable therefore, to make the beam size and the collector hole as small as possible. A series of measurements were carried out in attempt to find the optimum size. In Fig. 18 there is plotted, to the same scale, curves for two different values of s. In curve A the hole in the electron gun anode is .008" and the collimator hole is .0045". This corresponds to a total beam size of .017" with the center of the penumbra occurring at .013. The collector hole is .014" and the half width of the resulting peak is 28 volts. On the other hand in curve B the electron gun hole is .004" and the collimator hole is again .0045". This corresponds to a total beam size of .013 with the center of the penumbra occuring at .010. The collector hole used was .009" and the half-width is 17 volts. Now it will be noted that the half-widths of these two curves are in the ratio of 28/17 = 1.65; while the collector hole sizes are in the ratio of 14/9 = 1.55.

It is felt that the hole sizes used for curve B constitute a sort of practical limit. It is true that further decreases in hole size would lead to narrower peaks, but at the expense of current intensity with the attendant difficulties of measurement. Then too, as will be stated more fully later in section 3.7, the effect of charging at the holes becomes much more troublesome as the hole size is decreased.

3.3 General Considerations of Error.

In the sections that follow we shall discuss separately the various factors which contribute to the overall error of measurement. It is clear from the measured curves, however, that the error in the final measurement, from any and all causes, can be kept below one hundred parts per million. When our best curves were plotted to a very large scale, various "best choices" of the lines through the points gave V_o's at intersection which varied from one another in the case of the n = 4 curves for example, by only 0.1 volt in 1150. When it is considered that it should be possible by means pointed out below to reduce the scatter of the points considerably, a resolving power of one part in 10^4 does not seem at all optimistic.

We had of course, no way of checking on the reproducibility of V_o from curve to curve, but there is no theoretical reason to expect variations, and it is confidently expected that when accurate voltage measuring equipment is installed, no lack of repetition will be found. It seems that if the scatter of points is kept to a minimum that it is possible to resolve 1/100 th of the half-width of a peak.

3.4 Errors Due to the R. F. System.

The precision with which the resonant frequency of the cavity itself can be measured is not at present known. It should be possible by standard methods easily to measure a frequency to one part in a million provided that the frequency is itself stable to that accuracy. But quite aside from the effect of stability on the frequency measurement, the stability of the R. F. system has a pronounced effect on the

resolving power. Clearly all of the points on a current peak, if they are to mean anything, must be taken at the same value of magnetic field strength, frequency, and relative phase of the two modes producing the rotating field. The 8529 Klystrons are extremely sensitive to anode voltage variations--such variation producing considerable phase shift. It was found possible to change the relative phase by 90° by changing the anode voltage by only 3%. It is true that phase variations tend more to affect the "wings" of the peak curve, but a large phase variation can, nevertheless, not be tolerated. The 6000 volt D.C. generator used for this anode voltage in intrinsically quite stable but is subject to slow drifts and must be periodically checked

The amplitude of each mode must also, of course, remain constant throughout a given measurement. The peak width is relatively insensitive to R.F. power variation, depending as it does on the square root of the R.F. power. In the table below are given half widths for n = 4 curves taken at different settings of the attenuator between the SRL-6 Klystron and the 8529 amplifiers

TABLE III.

Attenuator Setting (db)	Half-width (volts.)
8	12
12	15
16	18

The amplifier Klystrons are not linear in their output vs. input characteristic, and thus the db attenuator values above must not be taken as an accurate indication of the output power.

It was found that the SRL-6 Klystron becomes unstable if the atten-

uation is reduced below 8db. It may be possible by installing an automatic frequency control circuit, not only to operate at higher power and lower attenuation, but also to improve the inherent frequency stability of the overall R.F. system.

It is comforting to note that changes in R.F. power while affecting the resolving power, do not introduce systematic errors, Uncertainties in frequency do introduce systematic errors, but as pointed out above, it should be possible to determine and hold constant the frequency with high precision.

3.5 Errors due to electron beam.

The customary procedure in taking point measurements for a peak curve is to set the beam potential and read the collected current with the R.F. first off, then on, then off again. In this way, the effect of drifts in total emission are minimized. Nevertheless, the measurement of I/I_0 involves the major source of error in these measurements. The D.C. amplifier used employed a 20 microampere panel meter with a scale the linearity of which is good to perhaps 2%. Assuming that one could read this meter accurately to about $\frac{1}{4}$ of a scale division the error of reading may account for $2\frac{1}{2}$%. The ordinates of the points of the peak-curve could conceivably be off as much as 4%.

The beam potential was, as mentioned above, found to be subject to drifts. These drifts while slow enough not to be troublesome if the voltage was being measured absolutely could nevertheless, during the course of a long run (say 3/4 hour) have sufficient cumulative effect to make the peak curves slightly asymmetric. This potential supply will

hardly be suitable in its present form for the final measurement, and revisions are planned and in progress.

It is clear that since the purpose of the experiment is to measure the velocities of electrons corresponding to a given potential, that a spread in the initial velocities at the electron emitter will introduce error. The emitter is operated at a temperature of about 1000 °K and thus has an average spread in electron energies corresponding to about .17 volts [1]. It can be shown [2] that when the spread in electron energies is small compared to the half width of the peak curve, the effect is simply to round off the top of the peak but not to produce any shift of the center. Here the half widths are of the order of 50 times the thermal spread and the error introduced is thus an order of magnitude smaller than that which is significant in this measurement.

Another source of observational uncertainties is the geometrical alignment of the apparatus as a whole. As mentioned in section 1.7, it is necessary to place the final collimating hole at the exit to the cavity in order to avoid the displacement effect of the beam in the cavity. As long as the diameter of the beam entering the cavity is several times as large as the magnitude of this displacement, the collimating hole will lie within the umbra of the displaced beam and will thus be illuminated with the undisplaced beam intensity. If however, due to poor geometrical alignment the collimating hole lies in the penumbra, then the collected current is less than I_0 for two reasons--one the displacement effect already mentioned and the other of course, the true effect of the beam potential differing from V_0. As long as this decrement of the

---

1. Here the well known relation; mean energy = 2kT has been used.
2. See Appendix II.

current due to displacement is small and constant it is not serious, for it simply introduces a renormalization of all of the peak curves. To the extent that it reduces the current of course it also reduces the sensitivity at the collector, and, of course, if the geometry varies during a run the data are invalidated. It is possible by removing the collector hole by the technique referred to in section 2.4, to obtain good geometrical alignment; for, with the hole removed and the beam potential close to a peak, no change of collected current should occur when the R.F. is switched on and off. The alignment should be checked in this way before every run.

3.6 Errors Arising from the Measurement of Cavity Length.

It is intended that for the final measurement of e/m the length of the cavity will be measured with extreme precision by interferometric means. As pointed out in section 1.5, however, the fact that the magnetic fields bulge into the holes where the electrons enter the cavity must be taken into account. It appears that this effect will tend to increase the effective length of the cavity by perhaps 1% or so, and as the amount and effect of this bulging can be calculated to extreme precision it should introduce no systematic error. It is planned, however, to check the calculations experimentally by the following method. Additional spacing rings have been provided so that the length of the cavity can be changed. Since the same end plates are used, and since the frequency of the TM_{110} mode does not depend on the length of the cavity, any differences between e/m as measured for the two different lengths will give a direct measure of the bulging effect. It does appear, however, that the length measurements will not constitute the

limiting condition on the overall accuracy.

3.7 Errors due to Charging of Pinholes.

It has been found that after the electron beam is allowed to bombard a surface for any extended length of time (say 10 hours) that a deposit of insulating material builds up on the surface and becomes charged by the electron beam. At the anode of the electron gun this charged layer can become so thick that it can actually shut off the beam entirely. The effect is also serious at the collimating holes, for it has been observed that when the collimating hole becomes charged, the beam is both blown up in size and deflected in position. This condition does not introduce systematic error, but, clearly, if the beam size is increased for any reason the resolving power is correspondingly decreased. Then too, if the beam is deflected by the charged hole, it becomes increasingly difficult to center the beam on the collector hole, as changes in current intensity will cause the beam to wander around.

From the operational point of view therefore, it is essential that runs be made only when the holes are clean. Up to the present time, it has been the policy to clean the holes before each run. This necessitates letting the system down to air, however, and it would be very desirable to introduce some system for cleaning the holes inside the vacuum. It is possible that providing a filament from which gold could be evaporated onto the collimating holes would accomplish this purpose.

3.8 Discussion of the Ultimate Obtainable Accuracy.

The final measurement of e/m will, in addition to the resolving power of the apparatus, involve the measurement of a length, a voltage

difference, and a radio frequency. Of these the limiting factor is almost certainly the voltage. As pointed out in section 1.5, it is possible to eliminate the effects of contact potentials, thermal e.m.f.'s etc. provided that they are constant throughout a run by measuring not the voltage of a peak, but the voltage difference between two successive peaks. The voltages will be measured by setting up a precision voltage divider and comparing the divided voltage with the e.m.f. of a bank of standard cells which is owned by the Institute and has been calibrated at the National Bureau of Standards. The National Bureau of Standards considers this calibration to be reliable to 10 parts in a million, and this will set an upper limit on the precision of the measurement.

The limiting factor in a given measurement is set by the resolving power of the instrument. As stated above this should be at least 100 parts per million. If then systematic errors have been eliminated and the errors in a given measurement can be considered truly random in distribution, it should be possible to extend to the limit of the voltage measurement by taking sufficient numbers of readings to provide good statistical averaging.

3.9 Suggestions for Improvements on the Apparatus.

Many improvements have already been suggested in the sections above, but we summarize them here.

1. Elimination of drifts from the beam potential source.
2. An improved method of cleaning pinholes.
3. A device for monitoring the phase and amplitude of the R.F.
4. A detecting instrument whose scale is more extended.

APPENDIX I.

Calculation of the Heat Flow Problem in the Walls of the Cavity.

We shall calculate the flow of heat in the side walls of the cavity under the simplifying assumption that the curvature can be neglected and the problem solved as a two dimensional one. It shall further be assumed that thermal equilibrium has been established so that the temperature, T, obeys Laplace's equation

$$\nabla^2 T = 0$$

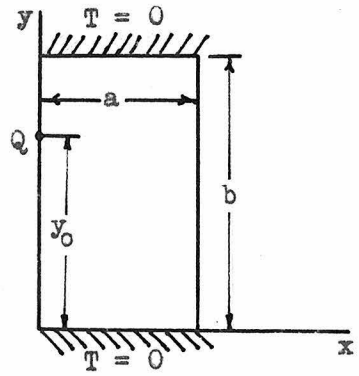

Fig. 19

In Fig. 19 at the left we have shown the coordinate system employed. We solve first for the temperature distribution when a unit source of heat is placed at $y = y_o$, $x = 0$, and shall then integrate this to obtain a uniform heat source distribution in y. The boundary conditions to be satisfied are $T = 0$, at $y = 0$ and at $y = b$; $\frac{\partial T}{\partial x} = 0$ at $x = a$ and at $x = 0$ except at $(x = 0 , y = y_o)$. We thus choose a particular solution of Laplace's equation

$$T = \sum_{n=0}^{\infty} A_n \left(\cosh\frac{n\pi a}{b} \cdot \cosh\frac{n\pi x}{b} - \sinh\frac{n\pi a}{b} \sinh\frac{n\pi x}{b} \right) \sin\frac{n\pi y}{b} \qquad \ldots(1)$$

which satisfies the boundary conditions at $y = 0$, $y = b$, and $x = a$. At $x = 0$ we write

$$\left.\frac{\partial T}{\partial x}\right|_{x=0} = \sum_{n=0}^{\infty} -A_n \frac{n\pi}{b} \sinh\frac{n\pi a}{b} \sin\frac{n\pi y}{b} \qquad \ldots\ldots(2)$$

We now multiply both sides of (2) by $\sin\frac{p\pi y}{b}\,dy$ and integrate between 0 and b. We obtain, using k for the coefficient of heat conductivity

$$\sin\frac{p\pi y_o}{b}\int_{\text{all } q}\left.\frac{\partial T}{\partial x}\right|_{x=0} dy_o \;=\; \frac{2\pi Q}{4\pi k}\sin\frac{p\pi y_o}{b} \;=\; -A_p\,\frac{p\pi}{b}\sinh\frac{p\pi a}{b}\int_0^b \sin^2\frac{p\pi y}{b}\,dy$$

Therefore, the coefficient A_p becomes

$$A_p \;=\; \frac{Q}{p\pi k}\,\frac{\sin\frac{p\pi y_o}{b}}{\sinh\frac{p\pi a}{b}} \qquad \ldots(3)$$

If we now let $Q \longrightarrow \frac{Q}{b}\,dy_o$, and $T \longrightarrow dT$, and integrate, we obtain for the case of uniform distribution of heat sources

$$T \;=\; \sum_{n\ \text{odd}} \frac{Q}{\pi n b k}\,\frac{2b}{n\pi}\,\frac{1}{\sinh\frac{n\pi a}{b}}\left\{\cosh\frac{n\pi a}{b}\cosh\frac{n\pi x}{b} - \sinh\frac{n\pi a}{b}\sinh\frac{n\pi x}{b}\right\}\sin\frac{n\pi y}{b}$$

where we have used the fact that $\int_0^b \sin\frac{n\pi y}{b}\,dy \;=\; \begin{cases} 0 \text{ for n even} \\ 2b/n\pi \text{ for n odd.} \end{cases}$

We shall calculate T at the point x = 0, y = b/2, for that point will be the hottest, and will show that the temperature rise is negligible. Now

$$T(x = 0,\ y = b/2) \;=\; \frac{2Q}{\pi^2 k}\sum_0^\infty \frac{(-1)^n}{(2n+1)^2}\coth\frac{(2n+1)\pi a}{b}$$

Let us now choose a/b = 3. This corresponds to the actual ratio of dimensions in the cavity. This means that all of the hyperbolic cotangents have large arguments and are essentially equal to unity. We obtain therefore, for T

$$T \;\approx\; \frac{2Q}{\pi^2 k}\sum 1 \;+\; 1/3^2 \;+\; 1/5^2 \;+\; 1/7^2 + \ldots$$

$$\approx\; \frac{2.4Q}{\pi^2 k} \qquad \ldots\ldots(4)$$

Now the heat conductivity of Molybdenum is .346 cal./cm.sec.deg., and we take as a pessimistic figure 40 watts as the amount of power dissipated in the cavity side walls. This gives Q = .3 cal./sec. cm. Putting these values into the expression (4) above gives

$T = 0.2\ ^{\circ}C$ temperature rise above the ends.

This rise will cause a negligible change in the cavity length. It will as pointed out in the body of the text however, be necessary to find the length of the cavity as a function of the temperature of the end plates.

Appendix II.

Effect of Thermal Electron Velocities on the Current Peak Shape.

It is of considerable interest to determine whether or not the thermal distribution of initial electron velocities seriously limits the accuracy with which the center of a current peak can be located. In order to calculate the order of magnitude of this effect, we assume that the peak in the absence of thermal velocities is ideal, i.e. sharp and symmetric when plotted on a voltage scale. On this ideal peak is superimposed the smearing effect of a thermal velocity distribution given by

$$N(u) = u \exp(-mu^2/2kT)\, du$$

This is the Maxwell-Boltzmann distribution which gives the fraction of the total number of emitted electrons which cross a surface with components of velocity perpendicular to that surface lying between u and u + du. In terms of voltage rather than velocity this distribution becomes:

$$N(u) = N(V) = \exp(-eV/kT)\, dV = \exp(-aV)\, dV$$

where we have used the abbreviation $a = e/kT$.

We desire to calculate the equation of the sides of the current peak; that is, we desire to find the current $I(V_0)$, as a function of the applied voltage V_0. It is therefore necessary to integrate the contributions to the current at V_0, coming from all the electrons which have higher energies. We shall explain the integrals which follow in terms of the notation introduced in Figure 20. The current $I(V_0)$, up to a normalizing factor, B, is given by the

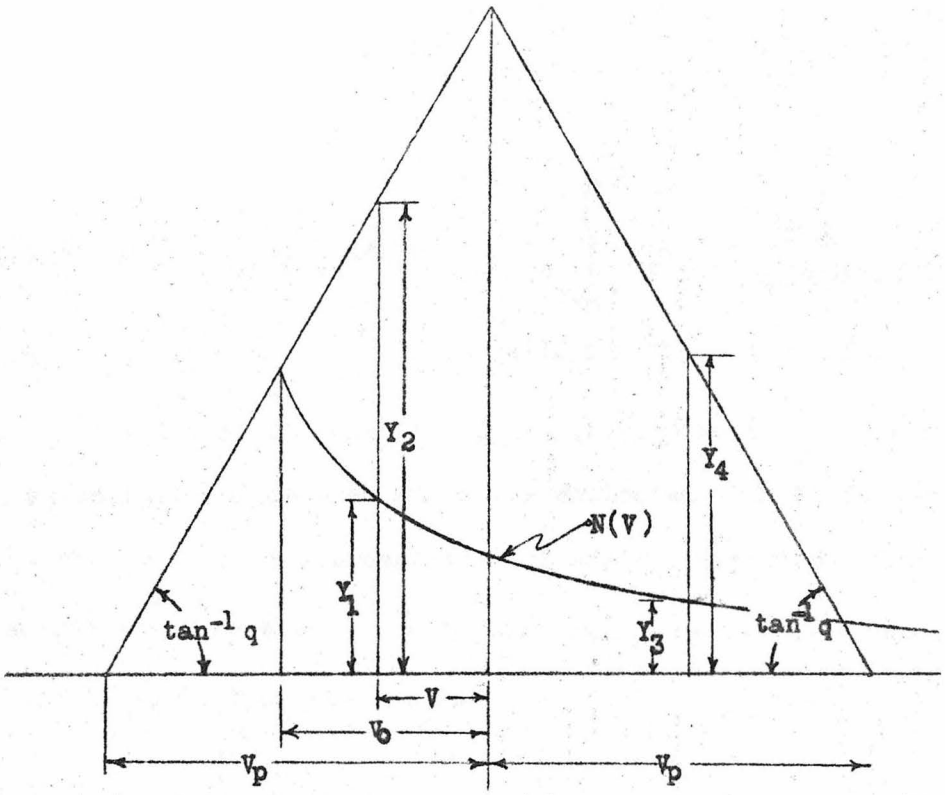

Figure 20.

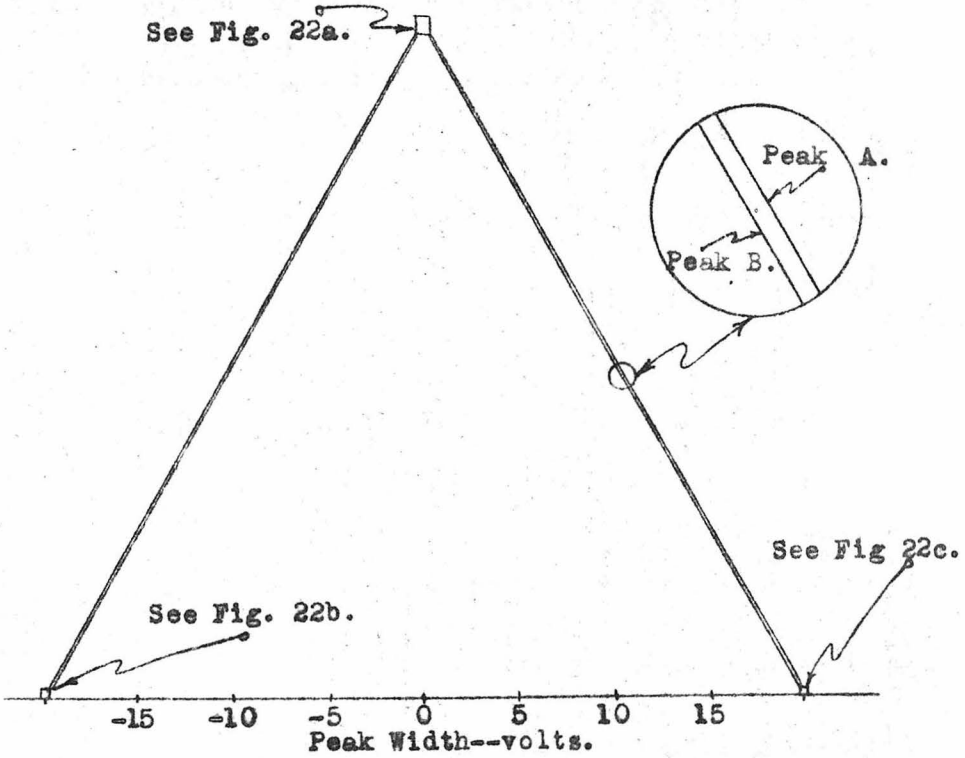

Figure 21.

following integrals

$$B\, I(V_0) = -\int_{V_0}^{0} Y_1 Y_2\, dV + \int_{0}^{V_p} Y_3 Y_4\, dV \qquad \ldots.(1)$$

valid for V_0 to the left.

where in the first integral for example, Y_1 is proportional to the fraction of electrons at voltage V from peak which are collected, and Y_2 is the factor which essentially gives the probability of their collection. These integrals describe the case when V_0 is to the left of center as shown in Figure 20. When V_0 is to the right we have

$$B\, I'(V_0) = \int_{V_0}^{V_p} Y_3 Y_4\, dV \qquad \ldots\ldots.(2)$$

valid for V_0 to the right.

From the definitions of Figure 20, these integrals can be written in the following form. Eq. (1) becomes, putting all constants into B:

$$B\, I(V_0) = -\int_{V_0}^{0} (V_p - V) \exp(aV - aV_0)\, dV + \int_{0}^{V_p} (V_p - V) \exp(-aV - aV_0)\, dV \qquad \ldots.(3)$$

Eq. (2) on the other hand, becomes

$$B\, I'(V_0) = \int_{V_0}^{V_p} (V_p - V) \exp(aV_0 - aV)\, dV \qquad \ldots.(4)$$

All of these integrations are elementary. Carrying out the integrations in Eq.'s (3) & (4), we obtain

$$B\, I(V_0) = \frac{V_p - V_0}{a} + \frac{1 - 2\exp(-aV_0) + \exp(-aV_p + -aV_0)}{a^2} \qquad \ldots(5)$$

The normalizing factor B is chosen to be $B = 1/qa$, because as $a \to \infty$, $I \longrightarrow q(V_p - V_o)$. This normalization gives

$$I(V_o) = q(V_p - V_o) + \frac{q}{a}\left[1 - 2\exp(-aV_o) + \exp(-aV_p - aV_o)\right] \quad \ldots(6)$$

Similarly,

$$I'(V_o) = q(V_p - V_o) - \frac{q}{a}\left[1 - \exp(aV_o - aV_p)\right] \quad \ldots.(7)$$

Now putting in the values $e = 1.6 \times 10^{-19}$ coulomb, $k = 1.4 \times 10^{-16}$ erg/degree, and using $T = 1000\ ^oK$, we find that $a = 10$. This is a very large value in all exponents and thus when V_o is neither, very close to 0 nor very close to V_p, all of the exponential terms are negligible and the current is shifted up in the case of I, and down in the case of I' by the amount q/a. Essentially this means that the original ideal peak is shifted to the left. This situation is illustrated in Fig. 21 where a peak of half-width 10 volts is shown. In this case $q = \frac{1}{2}/10 = 1/20$ and the voltage shift is given by

$$\Delta V = \Delta I/q = 1/a = 1/10 \text{ volt}$$
$$\Delta I = q/a = 1/200\ I_o$$

The effect of the thermal distribution near the peak and near the wings of the peak has been calculated from (6), and (7) above and is shown in Fig. 22 a,b,&c. respectively. Note that V above is independent of q, except near the top and at the wings and that therefore the voltage shift is the same for peaks of differing slopes. This means that the n = 3 say and n = 4, peaks are shifted by the same amount which will cancel when voltage differences are taken. The thermal distribution therefore, can be treated as just one more constant cancelling e.m.f.

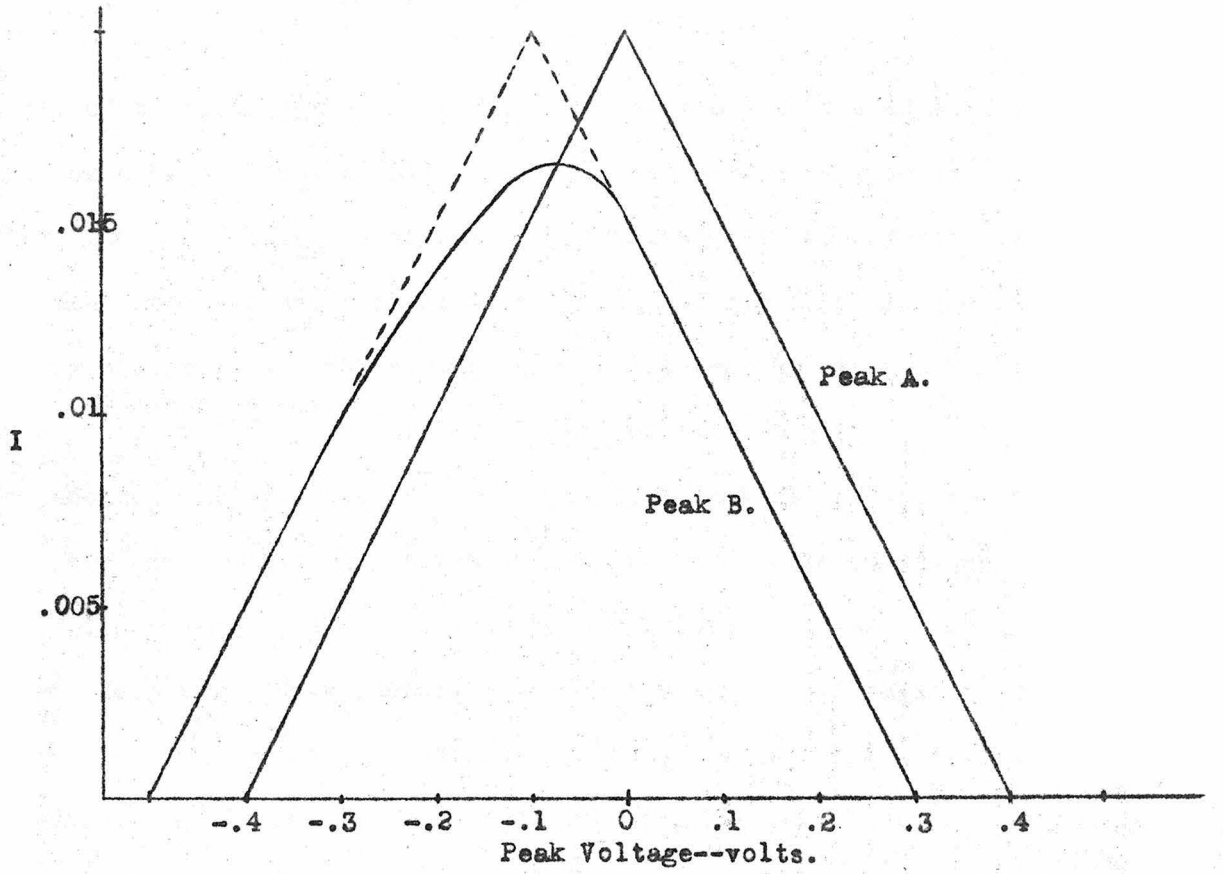

Figure 22a.

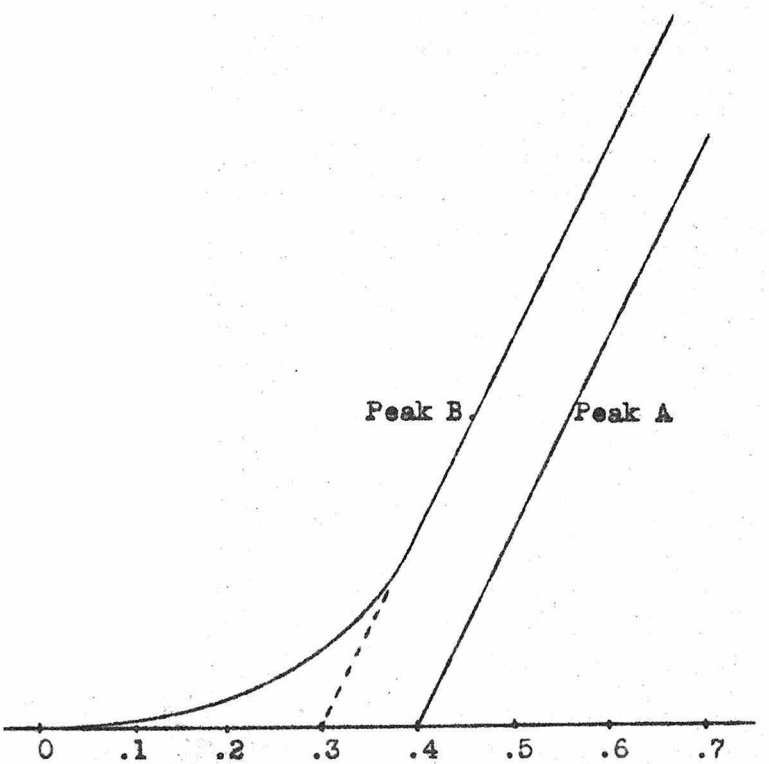

Figure 22b.

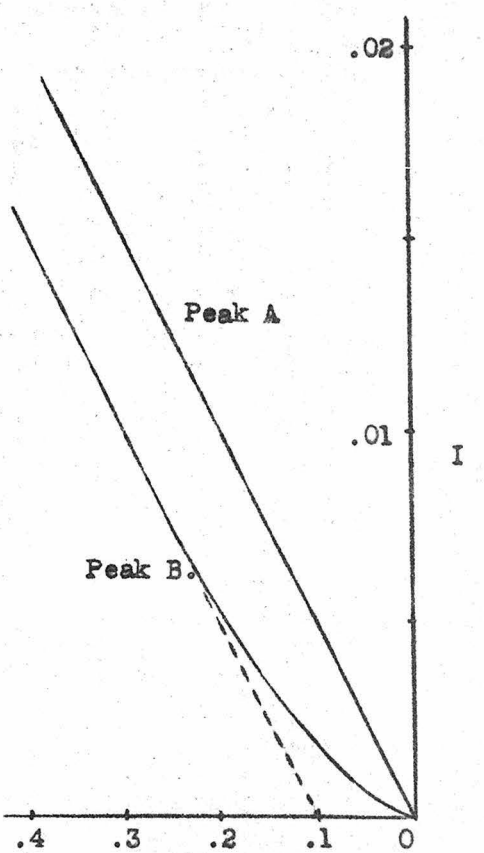

Figure 22c.

In all of the diagrams of Fig. 22, curve A refers to the ideal peak that would be obtained if all of the electrons were emitted at zero velocity, and curve B is the actual peak obtained if thermal velocities are taken into account. It is interesting to note by comparing Fig.22b and Fig 22c. that on the leading edge of the peak an exponential rise takes place, while on the trailing edge the current goes rigorously to zero when $V_o = V_p$. This is due to the fact that all of the electron velocities due to thermal agitation are in the forward direction, and add to the energy imparted to them by the voltage applied. Thus in Figure 22b., we can say that even though the applied voltage is too small to put us on the peak, nevertheless, some current will be collected. The integrals used in calculating Fig. 22b though not shown are very similar to Eq. (3)., and the integration is straightforward. It should be pointed out that the above calculations are valid for the case when the emission is temperature limited. It is customary to operate the electron source under these conditions.

APPENDIX III.

Table of Symbols Used in the Text.

a	radius of cavity exponent in Maxwell-Boltzmann distribution.
b	cyclotron frequency of the electron
B	magnetic flux density normalizing factor
c	velocity of light
d	length of the cavity
D	beam drift distance
e	charge on the electron
E	electric field intensity
f	frequency
g	dimensionless parameter--non-rotating field case
I	collected beam current--r.f. on
I_o	collected beam current--r.f. off
k	effective synchronous frequency Boltzmann constant heat conductivity
m	mass of the electron
P	power
q	see Fig. 20
Q	dimensionless cavity parameter magnitude of heat source
r	radius of the deflected beam
R	amount of beam deflection after drifting
s	width of slit or pinhole
t	time

T	period of the R.F temperature
u	thermal velocity
v	velocity of electron
V	voltage
w	$(2/T)\pi = 2\pi f$
x	rectangular cartesian coordinate
y	rectangualr cartesian coordinate
Y_i	See Figure 20.
z	rectangular cartesian coordinate cylindrical coordinate
α	beam deflectionangle--rotating case
β	wave number
γ	r.f. conductivity
δ	skin depth
θ	non-integral part of transit time--non-rotating case
μ	permeability
ρ	cylindrical coordinate
τ	transit time
ϕ	cylindrical coordinate phase of electron entry -- non-rotating case.